L/H Transition Characteristics due to Bipolar Losses in Tokamak Plasmas

Toda, Shinichiro
Interdisciplinary Graduate School of Engineering Sciences, Kyushu University

Yagi, Masatoshi
Research Institute for applied Mechanics, Kyushu University

Ito, Sanae-I.
Research Institute for applied Mechanics, Kyushu University

https://doi.org/10.5109/6786357

出版情報：Reports of Research Institute for Applied Mechanics. 44 (116), pp.55-85, 1998-10. 九州大学応用力学研究所

L/H Transition Characteristics due to Bipolar Losses in Tokamak Plasmas

By Shinichiro TODA*1, Masatoshi YAGI*2 and Sanae-I. ITOH*2

The L/H transition theory is extended based on the electrostatic bifurcation. We study the bipolar losses which have not been examined as the transition mechanisms yet and investigate the L/H transition characteristics. The comparison study with the experimental results is also done.

It is found that the equation of motions has the solutions with various hysteresis types of electrostatic bifurcation phenomena when the mechanisms of bipolar losses are considered. The dependences of the particle flux and the diffusivity on the thermodynamic force in the presence of the electric field are examined.

ELMs (Edge Localizes Modes) phenomena which are typical in the H-mode are studied. The model equation is newly extended to include the effect of the electric field shear in addition to the electric field shear. This model is also extended to the dynamic model which includes the temporal evolution of the density from the static model with the hysteresis characteristics.

Key Words: Tokamak, L/H transition, Radial electric field, Edge localized mode

1. Introduction

To utilize the released energy from the controlled thermonuclear fusion is a candidate as a new energy source of the next generations. The necessary temperature to attain the D-T reaction overcoming the Coulomb repulsion is about $10keV$. Since such high temperatures preclude the confinement by the material walls, Magnetic field is used to confine a plasma within a chamber without the contact with the wall. The tokamak, which was invented in U.S.S.R. in the mid-1960s, has been the most extensively investigated and advanced. In the tokamak reactor, it would be necessary to confine the energy of an enough dense plasma for a time which allows an adequate fraction of the fuel to react. The required ion density is around $10^{20}m^{-3}$ and the energy confinement time is of the order of a second, so-called 'break even condition'. It is just recently to reach the boundary of the break even in tokamaks. This is because the anomalous transport causes the degradation of the energy confinement (low confinement mode). Indeed, both heating and confinement still present substantial research tasks. One promising scenario in the tokamak reactor is the operation in the improved confinement regime known as H-mode (high confinement mode). H-mode has been observed in the large divertor tokamaks [1, 2, 3] for the first time. It occurs spontaneously when the neutral beam power exceeds a certain threshold value. It was later found that a similar plasma behavior can be produced with various heating methods in the divertor and limiter configurations, *e.g.*, in the ohmically heated limiter plasma discharges applying sufficient voltage to a probe several centimeters inside the plasma [4, 5, 6]. The onset of the H-mode is characterized by a sharp reduction in the H_α (or D_α) radiation, indicating a large reduction in recycling, and the sudden appearance of a strong radial electric field. The radial electric field seems to occur simultaneously with the suppression of the turbulent fluctuations. The improved confinement takes place before the pressure profile has changed significantly [7]. This suggests that the change in field in the cause, rather than the effect, of the improvement. The change is most prominent near the edge and

*1 Interdisciplinary Graduate School of Engineering Sciences, Kyushu University

*2 Research Institute for applied Mechanics, Kyushu University

referred to a transport barrier. The H-mode is generic nature of the high temperature plasmas in tokamaks. The physical issue of the L/H transition as the anomalous transport should be understood.

To understand the L/H transition, several possible explanations have been reported for the spontaneous H-mode transition (see, *e.g.*, Refs. [8, 9, 10, 11, 12, 13, 14]). Theories of H-mode were developed based on static and zero dimensional (0-D) model equations. A first theory based on the bifurcation of the radial electric field E_r was proposed. This theory provides a picture of the bifurcation of the transport coefficient and the establishment of the transport barrier. In H-mode regime, the radial electric field is likely to take a large negative value or positive value near the edge, whose magnitude is given by $|X| \simeq 1$ ($X \equiv e\,\rho_{pi}E_r/T_i$, ρ_{pi}: ion poloidal gyroradius, T_i: ion temperature) [8]. Another model led that the critical ν_{*i} ($\nu_{*i} \equiv \nu_{ii}Rq/(v_{Ti}\,\varepsilon^{\frac{3}{2}})$, ν_{ii}: ion-ion collision frequency, R: major radius, q: safety factor, v_{Ti}: ion thermal velocity, ε: inverse aspect ratio, at which the poloidal flow velocity makes sudden change to the more negative value, is estimated to be unity, *i.e.*, $\nu_{*i} \sim 1$ [10]. In both cases, the ion orbit loss was taken as an example of bipolar losses. Presently, it can be said that the bifurcations with the hysteresis characteristics of E_r and the poloidal rotation are put on the solid basis of the H-mode physics. Because it is difficult to evaluate accurately the hot ion orbit loss and measure the profiles of the electric field and other parameters, it has not been possible to make a definitive comparison between theory and experiment. The hard type bifurcation is predicted from the stationary (ambipolar) condition. In this case, the loss flux (as well as the radial electric field, fluctuation level and so on) takes multiple (three) values at the certain values of the fixed gradients. The hard transition is characterized by the fast transition at the critical points, has hysteresis and can generate the limit cycle solutions. The flux which induces the radial electric field can be caused by several mechanism: ion loss cone [8, 10, 11], ion bulk viscosity [10, 11, 14, 15], anomalous loss (including Reynolds' stress) [8, 16], electron ripple loss [15], the external biasing [5], and so on. Other models of the L/H transition were presented based on the soft transition of the electric field shear [17, 18]. The balance between the ion bulk viscosity loss and the anomalous loss, which contains the anomalous shear viscosity, was discussed [16, 17, 18, 19]. In this case, the variation from the low confinement state to the high confinement state can occur by following a smooth change. The inclusion of E'_r effect on the ion loss cone and the anomalous loss gave the variety of the bifurcation [20].

Edge localized modes (ELMs) are regularly observed phenomena characterized by the sudden drop of the edge density or temperature with a burst of particles or heat during the H phase in tokamak plasmas. The ELMs usually follow the L-to-H transition and show a variety in the magnitude and frequencies of the bursts and appear in some restricted parameter space of the H-phase [1, 21, 22, 23, 24, 25, 26]. The phenomenological analysis has been done. In various tokamaks, at the threshold, a sequence of L-H-L transitions is observed prior to the final transition into the H-mode [21, 22]. This phenomenon, a kind of ELMs, is known as a self-generated oscillation and is called "dithering ELMs". There are other class of ELMs (giant ELMs) which have large ampli -tudes. They are considered to appear when the edge plasma parameter is close to the critical stability value of the ideal MHD mode [2, 22, 24, 25, 26]. Based on the bifurcation theory of the multivalued curve of the poloidal rotation (or the radial electric field), a new model theory [27, 28] of dithering ELMs observed in JET-2M [21] was proposed. The model theory extended the zero-dimensional model of the L/H transition and included the temporal evolution and spatial diffusion. The equations for the edge density and the radial electric field of this theory are of time-dependent Ginzburg-Landau type. This theoretical model predicted periodic bursts of the loss flux (a self-generated oscillation) owing to the hysteresis curve in the transport coefficient as a dynamic solution. The parameter space for the occurrence of self -generated oscillation was obtained. The L/H transition has been observed to have the hysteresis characteristics of the plasma gradients and the associated flows of particles and heat [22, 25]. The existence of the self-generated oscillation was confirmed by ASDEX-Upgrade experiments [29]. The extended analyses on the coupled equations were done. The physical mechanism which involves the hysteresis was confirmed experimentally. Other models of ELMs were presented based on the soft transition of the electric field shear [17, 18]. How the effects of E'_r on anomalous loss influence the dynamics of the transition, *e.g.*, the dithering ELMs is necessary to study.

In this article, Chapter 2 surveys the L/H transition and ELMs physics base on former theoretical and experimental results. In Chapter 3, models of torques which may affect the momentum balance are listed. These models belong to the bipolar losses, which are the loss cone loss of ions, the bulk viscosity loss of ions, the hot ion loss due to the toroidal rippled field, the loss due to the collision between the neutral particle and the ion and the anomalous loss. Throughout Chapters 4, 5, 6, 7, using the poloidal rotation balance equation, the conditions for the L/H transition in the presence of the listed torques are newly examined. In Chapter 4, the effect of the hot ions on the L/H transition is studied to explain the experimental results in JT-60U. In Chapter 5, the impact of the bulk viscosity loss is examined and a new type of hysteresis characteristics is found. We name it 'double hysteresis characteristics'. This hyster-esis is found in a certain parameter region. The parameter region is clarified. Due to the double hyster-esis characteristics, the new-typed ELMs are found and investigated in detail. In Chapter 6, the research for the role of neutral particles on the L/H transition is done to study the experimental results of JFT-2M. Confirming the conventional knowledge that the neutrals at the main plasma mask the L/H transition, we find a new effect of neutrals. Namely, neutrals which are condensed near the X-point of the separatrix can induce the L/H transition. The comparison study is also made. In Chapter 7, the E'_r effect is examined explicitly in the bipolar losses. The E'_r effect is also included in Chapters 4, 5, 6, however, implicitly. The transition dynamics associated with the hysteresis curve is also investigated. The model theory for the ELMs is extended to include the effect of the radial electric field shear. From the static L/H transition model in the presence of the radial electric field shear, a model S curve for the diffusion coefficient versus the density gradient is formulated. The existence of a limit cycle solutions is confirmed in the presence of the radial electric field shear as well as the radial electric field. The summary and discussion are given in Chapter 8.

2. Reviews

The difference in energy confinement is the most important aspect of an H-mode plasma compared with an L-mode plasma [22]. The improvement of the global energy confinement time is due to a reduction of the electron heat diffusivity and the particle diffusion coefficient. The different energy and particle confinement properties L- and H-mode are clear from the differences in the plasma poloidal beta β_p and in the line averaged density $\bar{n}_e$ during the neutral injection (NI). Figure 1 shows the variation of H_α radiation in the divertor chamber. H_α increases during the L-mode and drops sharply at the L-H transition. In an H-mode, the particle content of the plasma rises sharply without external gas feed. The improved energy confinement causes the energy content of the discharge to rise, as is obvious from the diamagnetic signal. (See $\beta_{p\perp}$ in Fig.1.) The energy content of an H-mode plasma is nearly twice as large as that of an L-mode plasma, since the heating power is the same in the two cases and the energy confinement time in the H-mode is nearly twice as long as that in the L-mode. The variation of the edge electron temperature with the beam power in the limiter discharges is compared with that in L- and H-type divertor discharges. Almost a linear increase of T_e with P_{NI} is observed for the L- and H-type divertor discharges, where T_e is the electron temperature and

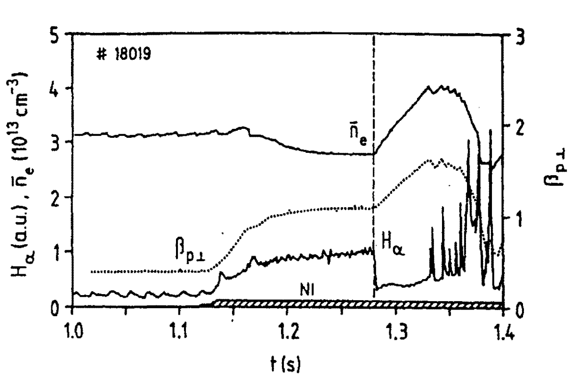

Fig. 1 Electron density $\bar{n}_e$, $\beta_{p\perp}$ and H_α radiation in the divertor chamber; the L/H transition is indicated by the dashed vertical line. (cited from Ref. [22])

P_{NI} is the power of the neutral injection. These experimental observations predict that the L-H transition can be viewed as a bifurcation phenomenon in the sense that the properties of the final state (*e.g.* the confinement properties) differ widely and also suggest that the transition should have a property that the heat and particle fluxes have two or multiple values for one condition of the temperature and density. The radial electric field, E_r, plays the role to cause such a transition as a hidden variable.

The prominent characteristic of H-mode is the formation of the transport barrier. That leads to reduced outflow of energy and particles, improved confinement properties of the plasma and steep gradients at the plasma edge with subsequent occurrence of ELMs. The drastic changes of plasma profile at the edge as monitored by SX diagnostic are shown in Fig.2. The SX radiation is given by the product of certain functions of n_e and T_e, where n_e is the electron density. A steep electron pressure gradient causes strong radial variation of the SX radiation. The profiles of Fig. 2 have been obtained just before L-H transitions and 50*ms* thereafter [22].

The experimental characterization of ELMs has

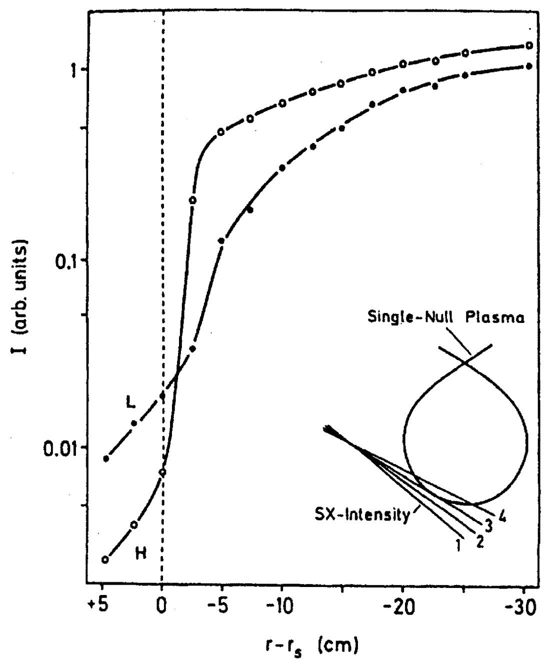

Fig. 2 Radial profiles of the SX radiation in the L-phase before the L-H transition and shortly afterwards at Δt=50*ms* (cited from Ref. [22])

recently began. For example, the classification of ELMs in ASDEX-Upgrade was made [30]. At a heating power near the power threshold for the L-H transition, periodic L-H-L transitions known as self-generated oscillation occur. For $(P-P_{sep}^{LH})/P_{sep}^{LH}>0.2$, ELMs called type III occur, where P is the injected power and P_{sep}^{LH} is the threshold power value of the L/H transition. They are characterized by $d\nu_{ELM}/dP<0$, where ν_{ELM} is the frequency of ELMs. The frequency decreases as the power is increased. For $(P-P_{sep}^{LH})/P_{sep}^{LH}\geq 0.5$, the discharge becomes ELM-free. ELMs called type I occur, for $(P-P_{sep}^{LH})/P_{sep}^{LH}\geq 1$. They are characterized by $d\nu_{ELM}/dP>0$. The power dependence of the frequency is opposite to that of type III. These ELMs are considered to appear when the edge plasma parameter is close to the critical stability value of the ideal MHD mode [22, 23, 24, 25, 26]. Comparison of the different dynamic behavior of the H-mode with varying $(P-P_{sep}^{LH})/P_{sep}^{LH}$ was shown in Fig.3. The new classification has been done recently in Ref. [31], considering the experimental results in the toroidal fusion devices in addition to ASDEX-Upgrade. Three distinct types of ELMs were listed there as follow:

1. *Dithering ELMs.* At $P_{sep}\approx P_{sep}^{LH}$, repetitive L-H-L transitions can occur, where P_{sep} is the energy power through the separatrix. Dithering cycles show no magnetic precursor oscillation. The level of turbulence during the temporary L-phase does not significantly exceed that of the L-phase at Psep $P_{sep}\leq P_{sep}^{LH}$.

2. *Type I ELMs.* The ELMs cycle frequency ν_{ELM} increases with the power in excess of P_{sep}, rather than P, *i.e.*, $d\nu_{ELM}/dP_{sep}>0$. There is a coherent magnetic precursor oscillation with toroidal mode number $N\approx 5-10$ and poloidal mode number $M\approx 10-15$ on the magnetic probes located close to plasma. A high level of magnetic fluctuations is detected during ELMs.

3. *Type III ELMs.* The ELM cycle frequency decreases with the power through the separatrix, *i.e.* $d\nu_{ELM}/dP_{sep}<0$. In present experimental results, there is no clear magnetic precursor oscillation. On the other hand, a high level of incoherent magnetic fluctuations has been detected.

To explain the experimental results, various kinds of theories for the H-mode transition were proposed. The first theory for the H-mode transition was reported [8] which included the bipolar loss in order to obtain the consistent ambipolar radial electric field. A bifurcation in the particle flux associated with the change of the radial electric field is found. By this theory, the particle and energy fluxes can have multiple values for the same density and temperature condition and the critical edge condition for the transition was obtained. The ion flux in the region of $|a-r| \leq \rho_{pi}$ is attributed to the direct orbital loss (a: minor radius, ρ_{pi}: ion poloidal gyroradius, $u_{Ti} m_i qR/(aeB_t)$, B_t: toroidal magnetic field). The ion orbital loss was given by

$$\Gamma_i = (n_i \nu_{ii}/\sqrt{\varepsilon}\,)\rho_{pi} F, \tag{2.1}$$

where the coefficient F is proportional to the relative number of particles in the loss cone in the velocity space, $0 < F < 1$ and n_i is the ion density. In order to estimate F in the presence of E_r, two simple assumptions were made. (1) The ions which satisfy the resonance condition $v_{\parallel}/(qR) = E_r/(rB_t)$ are lost directly. (2) The ion distribution function f_i is close to the Maxwellian, $f_i \propto \exp\,(-v^2{}_{\parallel}/v_{Ti}^2)$. Then the estimation $F \propto \exp\,\{-(\rho_{Pi} eE_r/T_i)^2\}$ was made and the ion loss has the form

$$\Gamma_i^{lc} = \frac{n_i \nu_{ii} \rho_{Pi} \hat{F}}{\sqrt{\varepsilon}} \exp\left\{-\left(\frac{e\rho_{Pi} E_r}{T_i}\right)^2\right\}, \tag{2.2}$$

where the coefficient $\hat{F}$ is the contribution of the bounce average. On the other hand, the anomalous loss was taken as

$$\Gamma_{e-i}^{anom} = -D_{e0}^{b} n_e \left(\frac{n'_e}{n_e} + \alpha \frac{T'_e}{T_e} + \frac{eE_r}{T_e}\right), \tag{2.3}$$

where α is a numerical coefficient of the order of unity. The parameter D_{e0}^{b} is the bipolar anomalous diffusivity. The prime denotes the derivative with respect to the radial direction. Equating Eqs. (2.2) and (2.3), the equation to determine the ambipolar electric field was given as

$$\exp\left\{-\left(\frac{e\rho_{Pi} E_r}{T_i}\right)^2\right\} = d_0 \left\{\lambda - \left(\frac{e\rho_{Pi} E_r}{T_i}\right)\right\} (\equiv \hat{\Gamma}), \tag{2.4}$$

where $d_0 = D_{e0}^{b} \sqrt{\varepsilon}/(\rho_{pi}^2 \hat{F} \nu_{ii})$ and $\lambda = -\rho_{pi}\,(n'_e/n_e + \alpha$

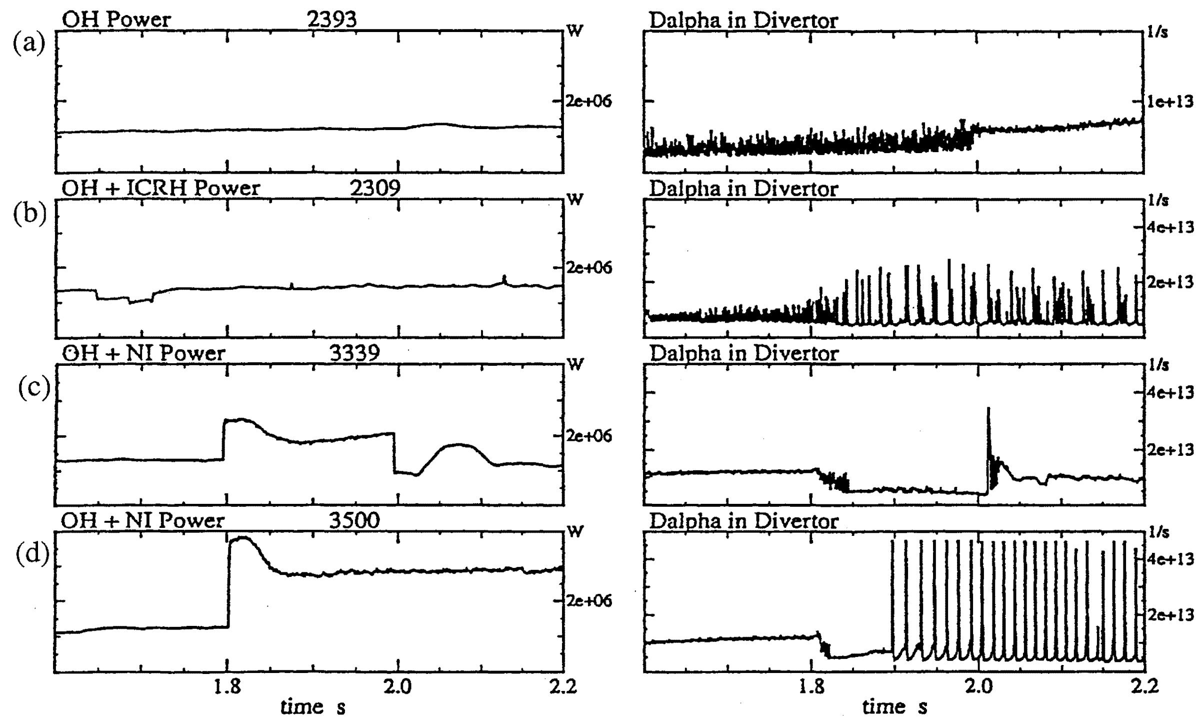

Fig. 3 Comparison of the different dynamic behavior of H-mode with varying $(P-P_{sep}^{LH})/P_{sep}^{LH}$, (a) $(P-P_{sep}^{LH})/P_{sep}^{LH} \approx 0.0$, (b) $(P-P_{sep}^{LH})/P_{sep}^{LH} \approx 0.2$, (c) $(P-P_{sep}^{LH})/P_{sep}^{LH} \approx 0.5$, (d) $(P-P_{sep}^{LH})/P_{sep}^{LH} \approx 1.2$, (cited from Ref. [30])

T'_e/T_e). Figure 4 (a) illustrates the λ dependence of $\hat{\Gamma}$ as the solution of Eq. (2.4) and Fig.4 (b) shows the λ dependence of the radial electric field. When λ is below the critical value λ_c, the electric field is negative and the fluxes are large. If λ exceeds λ_c, the electric field turns to positive and the fluxes are reduced. The L mode corresponds to the branch of the large loss flux and the H mode is the reduced loss flux. It is shown that the bifurcation from the L to H mode takes place as $A \to B' \to C \to C' \to D$ and that from the H to L mode occurs at $D \to C' \to B \to B' \to A$. Because λ_c, for the L- to H-mode transition is larger than that for the H- to L-mode transition, there is a hysteresis in the relation of $\hat{\Gamma}$ and λ as shown in Fig.4 (a). An extended model for the L-H transition was reported in Refs. [10, 11, 12]. The poloidal flow velocity U_p was chosen as an independent variable instead of E_r. To determine U_p, the poloidal momentum equation was solved. In standard neoclassical theory, the poloidal momentum is damped by the poloidal (parallel) viscosity $\langle \mathbf{B}_p \cdot \nabla \cdot \overleftrightarrow{\pi} \rangle$, because there is neither a momentum source nor a sink. Here $\overleftrightarrow{\pi}$ is the ion viscosity and the angular brackets denote the flux surface average. In the edge region, the poloidal rotation is driven by the torque or viscosity associated with the ion orbit loss or any other radial currents. The quantity $\langle \mathbf{B}_p \cdot \nabla \cdot \overleftrightarrow{\pi} \rangle$ was calculated by solving the drift kinetic equation with mass flow velocity [32]. The results is

$$\langle \mathbf{B}_p \cdot \nabla \cdot \overleftrightarrow{\pi} \rangle = (\sqrt{\pi}/4)(\varepsilon^2/r) n_i m_i u_{Ti} B_t (I_p U_p + I_T U_{p0}), \tag{2.5}$$

where $U_{p0} = -\rho_i u_{Ti}(dT_i/dr)/T_i$ and ρ_i is the ion gyro-radius. The integrals I_p and I_T are defined as

$$\begin{Bmatrix} I_p \\ I_T \end{Bmatrix} = \frac{1}{\pi} \int_0^{\sqrt{\nu^{*}i}} dx \begin{Bmatrix} 1 \\ \left(\frac{5}{2} - x\right) \end{Bmatrix} x^2 \exp(-x^2) \int_{-1}^{1} d\left(\frac{v_{\parallel}}{v}\right) \times \left[1 - 3\left(\frac{v_{\parallel}}{v}\right)^2\right]^2 \frac{\nu_{*i}\varepsilon^{\frac{3}{2}}(\nu_T/(\nu_i\sqrt{x}))}{(v_{\parallel}/v + U_{p,m}/\sqrt{x})^2 + [\nu_{*i}\varepsilon^{\frac{3}{2}}(\nu_T/(\nu_i\sqrt{x}))]^2}, \tag{2.6}$$

where v is the particle velocity, $x = v/v_{Ti}$, $U_{p,m} = U_p B/(v_{Ti} B_p) + \lambda/2$ for the radial force balance and ν_T is the collision frequency for the anisotropy relaxation [33]. The ion orbit loss rate was estimated to be

$$\left(\frac{\partial n_i}{\partial t}\right)_{orbit} = -\frac{G n_i \nu_{ii}}{\{\nu_{*i} + (wU_{p,m})^4\}^{\frac{1}{2}}} \exp\left\{-[\nu_{*i} + (wU_{p,m})^4]^{\frac{1}{2}}\right\}, \tag{2.7}$$

where G is a geometric factor of the order of unity that depends on the detailed shape of the loss cone in phase space and w, a numerical constant, accounts for the orbit shape, such as orbit squeezing [34, 35]. A assuming $\Delta r \sim \rho_{pi}$ where Δr is the characteristic width over which the ion orbit loss is important and Γ_i^{lc} is the particle loss associated with the ion orbit loss, the ion orbit loss was estimated to be

$$\Gamma_i^{lc} = \frac{G n_i \nu_{ii} \sqrt{\varepsilon}\,\rho_{pi}}{\{\nu_{*i} + (wU_{p,m})^4\}^{\frac{1}{2}}} \exp\left\{-[\nu_{*i} + (wU_{p,m})^4]^{\frac{1}{2}}\right\}. \tag{2.8}$$

Equation (2.8) shows an extended form from Eq.

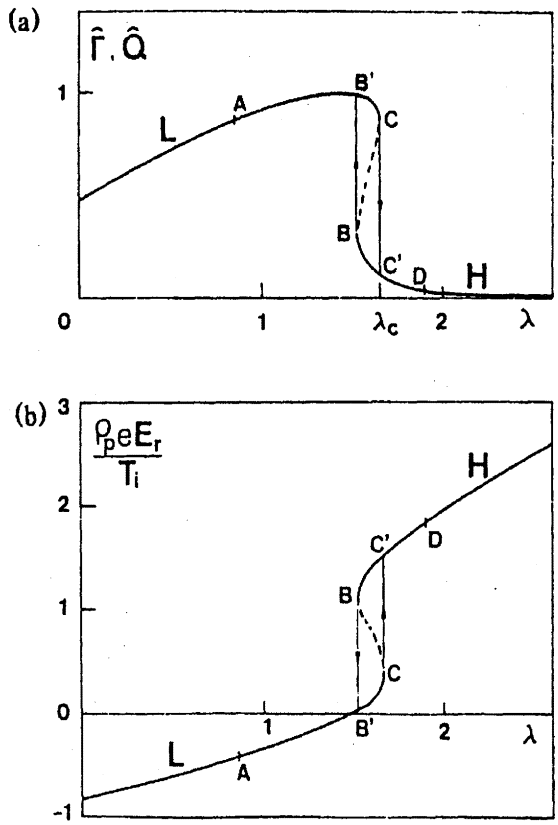

Fig. 4 Solutions for (a) the normalized flux and (b) the radial electric field as a function of λ (for the case of $d_0 = 1.3$). Transition from the branch of the large flux to that of small flux occurs as $\lambda = \lambda_c$. (cited from Ref. [8]

(2.2). The poloidal momentum balance equation leads

$$-(e/c)\Gamma_i^{lc}\times\mathbf{B}\cdot\mathbf{B}_p=\langle\mathbf{B}_p\cdot\nabla\cdot\overleftrightarrow{\pi}\rangle. \tag{2.9}$$

Substituting Eqs. (2.5) and (2.8) into Eq. (2.9), an algebraic equation for U_p was given as

$$\frac{G\nu_{*i}}{\{\nu_{*i}+(wU_{p,m})^4\}^{\frac{1}{2}}}\exp\{-[\nu_{*i}+(wU_{p,m})^4]^{\frac{1}{2}}\}=\frac{\sqrt{\pi}}{4}\left(\frac{\sqrt{\varepsilon}\,\rho_{pi}}{\Delta r}\right)\left[I_p\frac{U_pB_t}{v_{Ti}B_p}+I_tU_{p0}\right]. \tag{2.10}$$

The solution of Eq. (2.10) was obtained graphically by examining the intersections of two functions, $Y_1(U_{p,m})$ [the left hand side of Eq. (2.10)] and $Y_2(U_{p,m})$ [the right hand side of Eq. (2.10)] for a given set of parameters. As an example, parameters were set as follows: $G=1$, $(\pi\varepsilon)^{\frac{1}{2}}\rho_{pi}/(4\,\Delta r)=1.36$, $\varepsilon=0.25$, $w=0.5$, for simplicity, $\lambda=0.2$ and $U_{p0}B/(v_{Ti}B_p)=0.2$. The collionality ν_{*i} was chosen as the control parameter. As can be seen from Fig.5, at $\nu_{*i}=2.3$, there is only one solution of U_p. This solution was called the L root. At $\nu_{*i}=2.0$, there are three solution of U_p. The two outside solutions are stable and the one in the middle is unstable. The solution close to the origin is the continuation of the L root; the more negative stable solution is the new root (H root), which does not exist if there is no ion orbit loss. When ν_{*i} decreases further, only the more negative H root exists. In Fig.6, $U_{p,m}$ as the function of ν_{*i} was shown for the same parameters as in Fig.5. The critical ν_{*i} at which E_r makes a sudden change to a more negative was either greater than or less than unity. The different version of the ion loss due to the bulk viscosity was reported in Ref. [14]. The original neoclassical analysis by Galeev and Sagdeev [36] for the plateau and the banana regimes led to expressions for the particle loss due to the bulk viscosity of the form

$$\Gamma_j^{bv}=-D_j\left(\frac{n'_j}{n_j}+\gamma_j\frac{T'_j}{T_j}-\frac{e_j}{T_j}(E_r-B_pU_{j\parallel})\right)\exp\left\{-\left(\frac{e\rho_{pj}E_r}{T_j}\right)^2\right\}, \tag{2.11}$$

where $j=i$ or e denotes ions or electrons, respectively. In the plateau regime, $\gamma_j=3/2$ and $D_j=\sqrt{\pi}\,\varepsilon^2\rho_jT_j/(2re_jB_p)$, where $\rho_j=\sqrt{2m_jT_j}/(eB)$ is the Larmor radius, $U_{j\parallel}$ is the mean velocity along the magnetic field and the other notation is standard. For a plasma without an internal electrode, where neoclassical transport is the only source or loss mechanism, or if the other loss mechanisms are ambipolar, quasi-neutrality requires $\Gamma_i^{bv}=\Gamma_e^{bv}$. Since $D_e=O(m_e/m_i)^{\frac{1}{2}}D_i$, the first expression in brackets in the ion loss has to cancel to the same order, giving the ambipolar electric fields as

$$E_a=\frac{T_i}{e}\left(\frac{n'_i}{n_i}+\gamma_i\frac{T'_i}{T_i}\right)+B_pU_{i\parallel}. \tag{2.12}$$

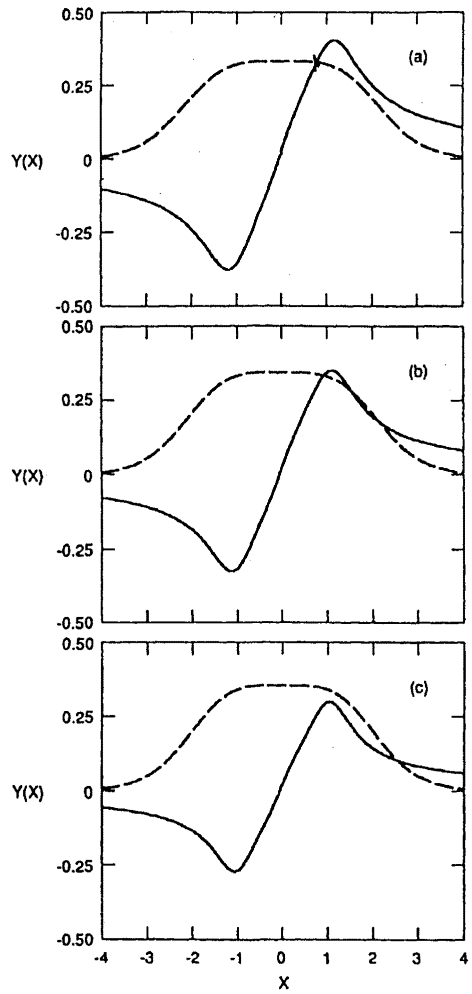

Fig. 5 The transition of $U_{p,m}\approx$X from (a) the L root to (b) the multiple root state and finally to (c) the H root as ν_{*i} decreases from 2.3 in (a) to 1.7 (c). The dashed lines are $Y_1(X)$ and the solid lines are $Y_2(X)$. (cited from Ref.[10])

It is frequently stated that neoclassical transport is intrinsically ambipolar. The argument for this is based on the flux surface averaged momentum balance. It leads to the same electric field, given by Eq. (2.12). This relation is used to eliminate E_r from Γ_e^{bv}, yielding an ambipolar loss which is independent of E_r. Although the ambipolar condition and the momentum balance give the same results when neoclassical transport is the only loss process, they may differ when another loss mechanism is present. If this other loss mechanism is not intrinsically ambipolar, then the ambipolar condition must be applied to the total particle flux, whereas the momentum balance argument claims that the neoclassical fluxes are separately ambipolar. As is discussed in Ref. [37], the momentum balance argument is valid only when there is no momentum source other than those of neoclassical processes. The same process which produces anomalous transport usually also produces anomalous momentum exchange, which should be included in the surface averaged momentum balance. In the presence of fluctuations, anomalous momentum loss must exist. Above discussions of the L-H transition was used a momentum balance argument. The first velocity moment of the kinetic equation gives a momentum equation in which kinetic effects such as Landau damping are included in a generalized pressure tensor. The two approaches, the arguments about the momentum balance and the kinetic equation, are equivalent. Considering Eq. (2.11), the radial ion loss can be written as

$$\Gamma_i^{bv}=\frac{\sqrt{\pi}\,\varepsilon^2 p_i}{eBr}(X-X_a)\exp(-X^2), \tag{2.13}$$

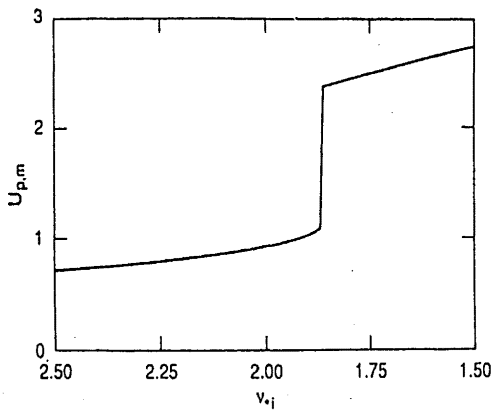

Fig. 6 The Change of $U_{p,m}$ as ν_{*i} decreases. (cited from Ref. [10])

where $X_a=e\rho_{pi}E_a/T_i$ and $p_i=n_iT_i$. The transition from the plateau regime to the collisional regime was studied by Connor and Stringer [38, 39], starting from the kinetic equation with a BGK collision operator. Connor and Stringer neglected the velocity dependence of the collision parameter, but this velocity dependence is not fundamental since a physical understanding is aimed here. This complete expression for the ion loss due to the bulk viscosity, given in Ref [39], which includes the effect of the poloidal electric field E_p, is long. In the following analysis, only the first term of this lengthy equation is used. The other terms, which result from E_p make a comparable contribution but do not change the asymp-totic behavior of the ion loss. (The effect of E_p was neglected by Galeev and Sagdeev [36] when deriving Eq. (2.11).) The radial ion loss due to the bulk viscosity was written in a form analogous to Eq. (2.13):

$$\Gamma_i^{bv}=\frac{\varepsilon^2 n_i T_i}{erB}(X-X_a)Im\ Z(X,\ y)+\Gamma_i^{P.S.}, \tag{2.14}$$

where

$$Z(X,y)=\frac{1}{\sqrt{\pi}}\int_{-\infty}^{\infty}\frac{\exp(-t^2)}{t-z}dt$$
$$=\exp(-z^2)\left(i\sqrt{\pi}-2\int_0^z\exp(t^2)dt\right), \tag{2.15}$$

$$z=X+iy,$$

$$y=\frac{r\nu_{ii}}{v_{Ti}\Theta}=\frac{qR}{\lambda_{mfp}},$$

$$\Theta=\frac{B_p}{B}$$

and λ_{mfp} is the mean free path defined as v_{Ti}/ν_{ii}. $Im\ Z(X,\ y)$ is tabulated by Fried and Conté [40]. The loss term $\Gamma_i^{P.S.}$, which is proportional to electron-ion frequency, is a generalization of Pfirsch-Schülter radial loss, valid for an arbitrary electric field. It is numerically small in all the applications of present interest and was neglected. Substituting Eq. (2.8) and Eq. (2.14) into Eq. (2.9), the argument was illustrated by Fig.7, which was a modification of Fig.5. The dashed line shows the current carried out of the plasma by those trapped ions whose orbits enter divertor or limiter shadow used in Eq. (2.8) with $w=0.25$. The solid line shows the ion current due to the bulk viscosity as given by Eq. (2.14), with its sign changed. The plasma collisionality parameter, qR/λ_{mfp}, decreases from (a) to (b) to (c). The ambipolar electric field, defined by $\Gamma_i^{lc}+\Gamma_i^{bv}=0$, was given by the intersection of the curves. Figure7 (a) represented an L mode plasma and showed that only one solution of ambipolar field was possible. In Fig.7 (b) there are three possible solutions for ambipolar fields, but the middle one is unstable. As the plasma evolves from condition (a) to condition (b), the electric field may be expected to continue at lowest ambipolar value of $|E_r|$. When the plasma moves into condition (c), this intersection disappears near the boundary and the electric field is forced to jump to further ambipolar value. This discontinuous jump in E_r is identified with observed sudden appearance of a strong electric field and a transition to H mode confinement. The various processes which can cause bifurcations have been reported.

If one writes the equation, for single charged ions, in terms of the electric field, one has

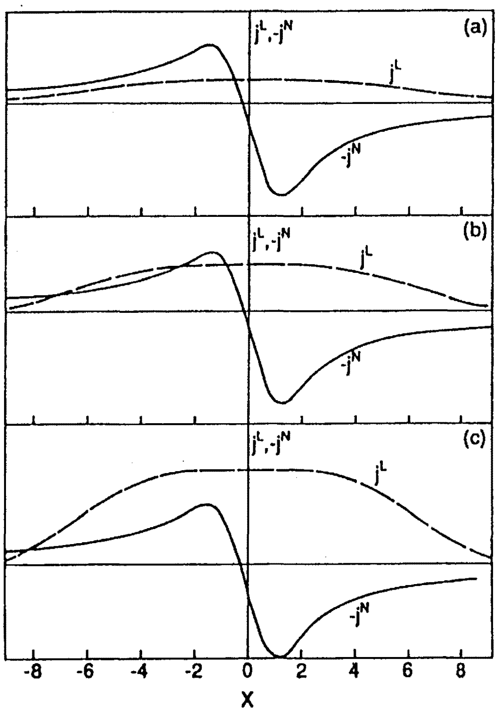

Fig. 7 Variation of the ion orbit and bulk viscosity loss currents with $X=e\rho_{pi}E_r/T_i$. The variables j^L and j^N represent the current due to the ion loss cone loss and the bulk viscosity loss, respectively. The parameter qR/λ_{mfp} decreases from (a) to (c). (cited from Ref. [14])

$$\frac{\varepsilon_0\varepsilon_\perp}{e}\frac{\partial E_r}{\partial t}=\Gamma_{e-i}^{anom}-\Gamma_i^{lc}-\Gamma_i^{bv}-\Gamma_i^{n}-\Gamma_i^{NC}+\Gamma_e^{NC}, \tag{2.16}$$

where ε_0 is the dielectric constant of the vacuum and $\varepsilon_\perp$ is the perpendicular dielectric constant of the magnetized plasma. The terms in the right hand side represent the following processes. The first terms in the right hand side represent the following processes. The first term, Γ_{e-i}^{anom}, is the contribution of the bipolar part of the anomalous cross field loss, which includes the Reynolds' stress term in the global flow. The second one, Γ_i^{lc}, is that from the loss cone loss of ions. The third, Γ_i^{bv}, is the one from the bulk viscosity, *i.e.,* due to the inhomogeneity of the magnetic field. The fourth term, Γ_i^{n}, is the loss of ions due to the collisions between ions and neutral particles. Others, Γ_i^{NC} and Γ_e^{NC} are from the contributions of other collisional processes. These terms have nonlinear dependence on the radial electric field and the balance between them allows the bifurcation. Combining the several terms in right hand side, the variety in bifurcation was predicted as above discussed. In the framework of zerodimensional analysis described above, the effect of the radial derivative of E_r, E'_r, was neglected. Actually, the radial derivative of E'_r is not negligibly small because E'_r is generated within the narrow region near the edge, in which the loss cone loss of ions exists. The characteristic thickness of the transition layer was predicted to be the width of a banana. Therefore the effects of E'_r on ion orbit and electron loss can be large than those E_r itself.

3. Model for bipolar losses

We first explain the model of bipolar flux driven by the five mechanisms. For the loss cone loss of ions, we employ the generalized form in Ref. [11]:

$$\Gamma_i^{lc}=\frac{n_i\nu_{ii}\sqrt{\varepsilon}\,\rho_{pi}}{[\nu_{*i}+U_{p,m}{}^4]^{\frac{1}{2}}}\exp\{-[\nu_{*i}+U_{p,m}{}^4]^{\frac{1}{2}}\}, \tag{3.1}$$

where ρ_{pi} is the ion poloidal gyroradius and E_r is the radial electric field. The other parameters are standard. We set $G=1$ and $w=1$, for simplicity.

Assuming $E_r=-U_p/B_p$ (U_p is the poloidal velocity of plasmas,) the model for the bulk viscosity loss of ions [11] due to the inhomogeneity of the magnetic field is rewritten as

$$\Gamma_i^{bv}=\frac{\sqrt{\pi}\,n_i\varepsilon^2\rho_{pi}}{4r}\left(I_p\frac{e\rho_{pi}E_r}{T_i}+I_t\frac{U_{p0}B}{v_{Ti}B_p}\right)\cdot v_{Ti}\frac{B_p}{B},\tag{3.2}$$

where $U_{p0}=-\varepsilon\rho_{pi}T'_i/(2qT_i)$ (the prime denotes the radial derivative.). The details about the integrals I_p and I_t are shown in Eq.(2.6). Equation (3.2) gives the values averaged over the magnetic field. The model of the hot ion losses due to the toroidal rippled field is intrinsically bipolar and is expressed [41] as

$$\Gamma_i^{rp}=-C_{rp}\delta^{1.5}\left(\frac{T_h}{eBR}\right)^2\frac{n_h}{\nu_{ih}}\left(\frac{n'_h}{n_h}-\frac{eE_r}{T_h}+3.37\frac{T'_h}{T_h}\right),\tag{3.3}$$

where $C_{rp}=12.38$, δ is the toroidal ripple and the subscript h represents the hot ion component. Equation (3.3) also gives the values averaged over the magnetic surface. The necessary condition for hot ions to satisfy the condition for ripple diffusion is given in the collisionless regime [41] as $\nu_{ih}<(\varepsilon\delta)^{0.75}v_{Ti}/R$.

Next we show the model of charge exchange loss between the ions and neutrals. With toroidal rotation, the collision process with neutral particles at the main plasma reduces the ion momentum without transferring it to the electrons. Due to this momentum imbalance, a bipolar loss of ions occur. The loss of ions due to the collision is employed as (See Ref. [9, 42])

$$\Gamma_i^{n}=-\frac{m_in_0\langle\sigma v\rangle n_iT_i}{(eB_p)^2}\frac{1+2q^2}{q^2}\left(\frac{n'_i}{n_i}+\alpha_i\frac{T'_i}{T_i}-\frac{eE_r}{T_i}\right),\tag{3.4}$$

where n_0 is the density of neutral particles, σ indicates the collision cross-section, so that $n_0\langle\sigma v\rangle$ stands for the rate of the collision. The symbol $\langle\ \ \rangle$ indicates the averaged quantity over the ion distribution. The numerical constant α_i is close to unity. The superscript n represents the loss due to the collision between the ions and the neutral particles.

The model for the anomalous bipolar loss has been discussed first in Ref. [8] and then by others in terms of the Reynolds' stress of turbulence [43]. It depends on both the electric field and its radial derivative (see a review [44] for the detailed description). In order to perform the point model for the dynamics, we introduce a simplification as $E'_r=E_r/\ell$ and express E'_r in terms of E_r in Fig.8. The typical length ℓ is further approximated as constant.

We have compared this zero-dimensional model to the accurate solution which was obtained by solving the spatial-temporal evolution, and found that the essential characters of the dynamics of dithering ELM are properly kept in this simplified model [45]. Based on this result, we here employ this constant-ℓ approximation in this analysis, and employ a simplified expression for the anomalous bipolar loss Ref. [8, 46] as

$$\Gamma_{e-i}^{anom}=-D_{e0}^{b}n_e\left(\frac{n'_e}{n_e}+\alpha\frac{T'_e}{T_e}+\frac{eE_r}{T_e}\right),\tag{3.5}$$

where D_{e0}^{b} is the bipolar part of electron effective diffusivity without considering E'_r explicitly and α is the coefficient of $O(1)$. The expression of Eq. (3.5) is a simplified model formula of the turbulent-driven contribution.

The radial fluxes of the electrons and ions near the plasma edge are studied in the presence of the electric field and electric field shear. The ion particle flux from the edge layer was calculated in Ref. [20] in the presence of the radial electric field shear. Considering the electric field shear, the banana width can be compressed [32] by the factor $1/\sqrt{|1-u_g|+C\varepsilon}$ [20], where $u_g=\rho_{pi}E'_r/(v_{Ti}B_p)$, ρ_{pi} is the ion poloidal gyroradius and the prime denotes the derivative with respect to the radial direction. The electric field shear squeezes (expands) the banana width. In the limit of $u_g\to 1$, the banana width reaches a maximum value. The numerical coefficient C denotes this corrections. By taking into account the u_g corrections, the ion loss has been given in the form as

$$\Gamma_i^{lc}=\frac{\hat{F}}{\sqrt{\varepsilon}}\frac{n_i\nu_{ii}\rho_{pi}}{\sqrt{|1-u_g|+C\varepsilon}}\exp\left[-\left(\frac{e\rho_{pi}E_r}{T_i}\right)^2\right],\tag{3.6}$$

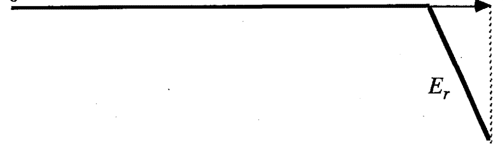

Fig. 8 The assumed radial electric field structure near the edge, by way of illustration. The radial extent of the transport barrier is expressed by ℓ and we assume ℓ to be constant.

where n_i is the ion density, ν_{ii} is the ion-ion collision frequency, T_i is the ion temperature and $\hat{F}$ is a numerical coefficient of the order of the unity. The superscript lc stands for the loss cone loss.

The electric field shear affects the microscopic stability and the anomalous flux. This has been studied and shown for the fluid turbulence of the edge plasma in the literature (see, *e.g.,* [11, 16, 17, 18, 19, 20, 47, 48, 49]). For simplicity, we examine the collisionless limit of the drift instability of trapped particles. We employ the expression of the bipolar part of effective diffusivity D_e^b in the presence of E'_r, given in Ref. [20] as

$$D_e^b=D_{e0}^b\sqrt{1+\frac{u_g}{u_c}}\,, \tag{3.7}$$

where D_{e0}^b is the difference in the bipolar parts of electron effective diffusivity and ion effective diffusivity due to this mode in the absence of E'_r. The factor $\sqrt{1+u_g/u_c}$ comes from the change of the banana orbit width owing to the change of toroidal precession frequency of trapped ions. The mode is stabilized if E'_r is negative and the condition $u_g<u_c$ is satisfied. The critical parameter u_c satisfies the relation $u_c^2=8\sqrt{2\varepsilon}(4-u_c)$ and is around 3 for the standard parameters. Based on this result in addition to the constant-ℓ approximation, the bipolar component of the fluxes near the edge is modeled as

$$\Gamma_{e-i}^{anom}=-D_{e0}^b\sqrt{1+\frac{u_g}{u_c}}n_e\left(\frac{n'_e}{n_e}+\alpha\frac{T'_e}{T_e}+\frac{eBr\hat{\omega}}{MT_e}\right). \tag{3.8}$$

In Eq. (3.8), M is the poloidal mode number and $\hat{\omega}$ is the angular frequency of the mode. In the presence of E_r, $\hat{\omega}$ is the Doppler shifted by ω_E as $\hat{\omega}=\omega+\omega_E$, where $\omega_E=ME_r/(rB)$. The superscript *anom* represents the anomalous loss and the coefficient α is the order of the unity.

4. Change in the H-mode dynamics due to ripple loss of fast ions.

4.1 Introduction

The regime where the L/H transition can occur was studied extensively. Investigation about the criterion of the L/H transition is not complete, but it is evident that the L/H transition can be more easily obtained above a certain density [22]. The H-mode in JT-60U with the neutral beam injection [50] showed a peculiar behavior. The L-to-H transition became rather unclear and the improvement of confinement became soft and continuous with power, which was observed in a low density plasma: $n_e=(2-3)\times10^{19}(m^{-3})$. On the other hand, the ELMy-H-mode appears in the high density regime. The ELMy-H-mode implies the hard typed L/H transition which has the hysteresis characteristics. We theoretically investigated this discharge and examined the ambipolar condition in detail. If $\nu_{*i}<<1$ holds (in large sized machine like JT-60U), the L-H transition without the hysteresis characteristics, namely soft transition, is predicted in the case $T_i=5(keV)$ and the low density [51]. In this situation the transition from the low confinement branch to the high one occurs by following the smooth change of the flux. Furthermore, our theory predicted the higher density makes the L/H transition harder. This prediction agrees with the experimental results. This transition theory may be a candidate to explain the unclear L/H transition and ELMy-H-mode in JT-60U. However, this previous analysis seems to be incomplete, since the ripple in JT-60U is large. Therefore, we need to study the behavior and loss processes of hot ions produced by neutral beam injection with a rippled toroidal field. Here we extend the bifurcation model to include the effects of the hot ion loss and examine the characteristics of the L/H transition in the typical parameters of JT-60U. The three bipolar losses are examined for the electric field and its shear. The contents of this chapter are reported in Ref. [52].

4.2 Ambipolar condition including Γ_i^{lc}, Γ_i^{rp} and Γ_{e-i}^{anom}

The ambipolar condition in consideration with Γ_i^{lc} (Eq.(3.1)), Γ_i^{rp} (Eq.(3.3)) and Γ_{e-i}^{anom} (Eq.(3.5)) is $\Gamma_i^{lc}+\Gamma_i^{rp}=\Gamma_{e-i}^{anom}$. This condition heads to

$$\frac{\nu_{*i}}{[\nu_{*i}+X^4]^{\frac{1}{2}}}\exp\{-[\nu_{*i}+X^4]^{\frac{1}{2}}\}+\frac{C_{rp}\delta^{1.5}}{\sqrt{\varepsilon}\,\omega_b}\left(\frac{T_h}{eBR}\right)^2$$

$$\frac{(1/r_n-1)}{\nu_{ih}\rho_{pi}^2}\left(\lambda_h+\frac{T_i}{T_h}X\right)=d(\lambda-X)/r_n(\equiv\hat{\Gamma}), \tag{4.1}$$

where $d=D_{e0}^b/(\sqrt{\varepsilon}\,\omega_b\rho_{pi}^2)$, $\lambda=-\rho_{pi}n'_e/n_e$, $\lambda h=-\rho_{pi}n'_h/n_h$, and $r_n=n_{i0}/n_i$ $(n_i=n_h+n_{i0})$. Here we assume $T_i=T_e(\equiv T)$, $n_i=n_e(\equiv n)$ and $T'=0$ for the analytic insight. We set $U_{b,m}=X$ for simplicity. We assume that the scale lengths of the density gradient of electrons and hot ions are equal, *i.e.*, $\lambda=\lambda_h$. The parameters used in the following calculations are similar to the JT-60U tokamak : major radius $R=3.03$ (m), minor radius $a=0.95\,(m)$, toroidal magnetic field $B_t=3.7\,(T)$, safety factor $q=3$, $D^b_{e0}=0.4\,(m^2/s)$ and $\delta=1\,(\%)$.

4.3 Characteristics modification of L/H transition due to hot ions

First the temperature $T_i=5\,(keV)$ and density $n=2.0\times10^{19}\,(m^{-3})$ are kept fixed. We investigate two cases of $r_n\,(=n_{i0}/n_i)=1.0$ (*i.e.*, no hot ions) and $r_n=0.98$ (the ripple loss exists) to examine the effects of the ripple loss on the L/H transition. In the case $r_n=0.98$, we set $T_h=50.0$ or 75.0 (keV). Figure 9 shows the normalized particle flux $\hat{\Gamma}$ v.s. the thermodynamic force λ as the solutions of Eq. (4.1). In this parameter regime, the ripple loss of hot ion is much smaller than other two losses at the neighborhood of the L/H transition. The ripple loss of hot ions makes the L/H transition softer than the case with only Γ_i^{lc} and Γ_e^{anom}. Moreover the jump of the flux at the L/H transition is predicted to be smaller (shallower transition) when the ripple loss of hot ions exists. When λ becomes large, the ripple loss is dominant compared to the loss cone loss of ions. Especially, the ripple loss is considerably large in the case $T_h=75.0\,(keV)$ since $\hat{\Gamma}_i^{rp}\propto T_h^{3.5}$ ($\hat{\Gamma}_i^{rp}$ is the second term in the left hand in Eq. (4.1)). Next we fix the temperature of the bulk ions as $T_i=5\,(keV)$ and set $r_n=0.98$ and $T_h=50.0\,(keV)$. Figure 10 shows the variation of the normalized particle flux $\hat{\Gamma}$ in Eq. (4.1) as the function of the thermodynamic force λ for the various values of the density. Also in this case the L/H transition becomes shallower due to the effect of the ripple loss. The hysteresis characteristic is obtained, especially in the case of the high density: $n=5.0\times10^{19}\,(m^{-3})$. This type of the transition (hard transition) theory predicts the existence of a kind of ELMs (the self-generated oscillation) at the neighborhood of the L/H transition. This prediction agrees with the experimental results in the high density regime [50]. The softer transition is obtained in the case of a low density: $n=2.0\times10^{19}\,(m^{-3})$ than in the case of the high density. This transition from the branch of the large flux (corresponding to L-mode) to that of the low flux (corresponding to H-mode) occurs gradually in the $\hat{\Gamma}-\lambda$ plane. This situation of the transition may correspond to the fact that the gradual improvement of the confinement continues with the injection of neutral beam. For the low density case, the jump of the flux in the L/H transition is found to become small and is a half of the case in the high density regime.

5. Double hysteresis in L/H transition and compound dithers

5.1 Introduction

The bifurcation theory of the radial electric field was presented for the L/H transition [8, 9]. This

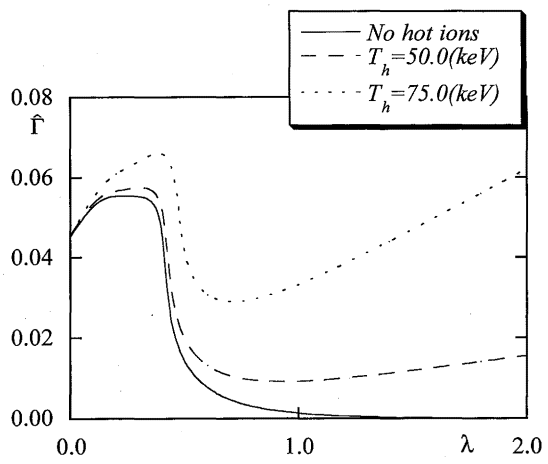

Fig. 9 The Change in the L/H transition due to the ripple loss of the hot ions. The ripple loss makes the transition softer.

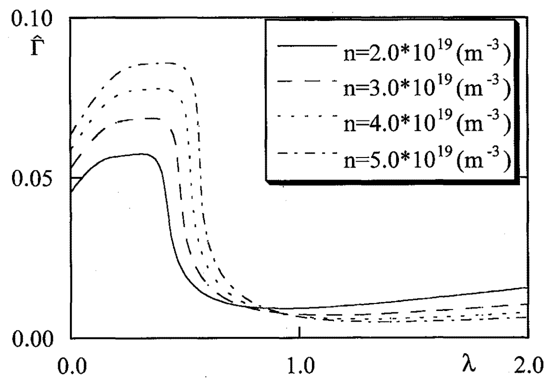

Fig. 10 The variation of the L/H transition for the various values of the density. For the low density, the soft typed transition is predicted. On the other hand, the hard transition is predicted in the high density.

model predicts the self-generated oscillation near the threshold condition for the transition [27], which was attributed to the model of dithering ELMs. Experimental study confirmed that this theoretical picture explains characteristic features of the dithering ELMs [29]. The bifurcation model was extended and many mechanisms have been proposed as an element to generate the radial electric field [43]. Among them the mechanism by the collisional bulk ion viscosity [11] was also considered to be important in experimental conditions (see, *e.g.,* Ref. [14]). We have compared the impacts from the mechanisms of the bipolar losses, *i.e.,* the loss cone loss, collisional bulk viscosity loss of ions and the anomalous loss, and found that these three could have comparable contributions for the parameters of $\nu_{*i}>0.1$ [51]. It is necessary to investigate what kind of dynamics is generated from the competition of these three important mechanisms. This would give a key to understand the complex features of ELMs in experiments, for which the understanding and control are urgent tasks. In this chapter, three mechanisms for the electric field and the electric field shear generation are simultaneously examined. It is found that, if ν_{*i} is of the order of unity, there exists the five-fold multiple states in the gradient-flux relation. Dynamics near the transition condition is analyzed by use of the point model in which the gradient length of radial electric field is treated as constant. The new compound limit cycle oscillation is predicted to occur. The contents of this chapter are reported in Ref. [53].

5.2 Double hysteresis in L/H transition

The ambipolar condition including Γ_i^{lc}, Γ_i^{bv}, Γ_{e-i}^{anom} is given by $\Gamma_i^{lc}+\Gamma_i^{bv}+\Gamma_{e-i}^{anom}$. Using the models of the bipolar losses, Eqs. (3.1), (3.2) and (3.5), this condition lead to

$$\frac{\nu_{*i}}{[\nu_{*i}+U_{p,m}{}^4]^{\frac{1}{2}}}\exp\{-[\nu_{*i}+U_{p,m}{}^4]^{\frac{1}{2}}\}+\frac{\sqrt{\pi}}{4}$$

$$(I_p(U_{p,m}-\lambda/2)+0.2I_t)=d(3\lambda/2-U_{p,m})(\equiv\hat{\Gamma}). \tag{5.1}$$

For simplicity, we set $n_e=n_i(\equiv n)$, $T_e=T_i(\equiv T)$ and $U_{p0}B/(v_{Ti}B_p)=0.2$. The parameters used in the following calculations are similar to those of JFT-2M tokamak: $R=1.3(m)$, $a=0.35(m)$, toroidal magnetic field $B_t=1.3(T)$ and safety factor $q=3$. We fix the density $n=1.0\times10^{19}(m^{-3})$ and the effective frequency $\nu_{*i}=2$. We investigate the competition between the three terms in Eq. (5.1) and obtain the bifurcation curve for various values of d. Figure 11 shows the dependence of the normalized particle flux on the thermodynamical force (gradient parameter) λ for $d=0.05$ ($D_{e0}^b=0.05(m^2/s)$) (Fig.11(a)) and for $d=0.1$ ($D_{e0}^b=0.1(m^2/s)$) (Fig.11(b)). The multiple bifurcation is demonstrated in the former case. In both cases, the hysteresis $D\to D'\to E\to E'\to D$ appears, as has been found in Refs. [8, 9] where the second term in Eq. (5.1) has been neglected. If the anomalous loss is small, then the contribution of the second term increases, so that the new hysteresis ($B\to B'\to C\to C'\to B$) is generated combined with the other hysteresis. The double hysteresis appears. As was the fundamental cusp, this bifurcation has the nature of the cusp-type catastrophe; it disappears if d is enhanced and the second term in Eq. (5.1) becomes loss important (Fig.11(b)). The L-mode corresponds to the branch of the large loss flux and the H-mode is the branch of the reduced loss flux. For an adequate

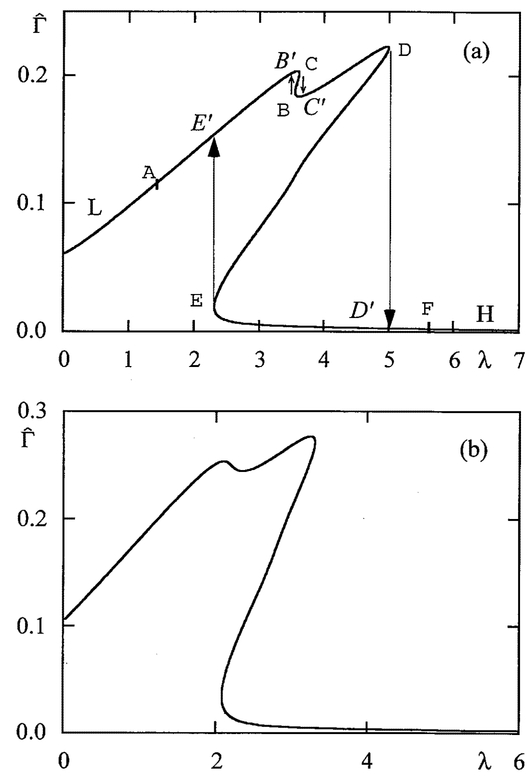

Fig. 11 The solutions of Eq. (5.1) in $\hat{\Gamma}-\lambda$ plane in the case of (a) $d=0.05(D_{e0}^b=0.05)$ and (b) $d=0.1(D_{e0}^b=0.1)$.

influx exists, the transition from L-mode to H-mode takes place as $A \to E' \to B' \to C \to C' \to D \to D'$ and from H-mode to L-mode occurs at $F \to D' \to E \to E'$. However, in the case of the other value of the influx ($\hat{\Gamma} \sim 0.2$), the transition occurs as $A \to E' \to B' \to C \to C' \to B \to B'$. Temporal evolutions of the particle flux are discussed in the next section in two cases of influxes.

5.3 Time evolution and compound dithers

We investigate the dynamics of the H/L transition by choosing two dynamical variables, *i.e.*, the pressure gradient parameter λ and the effective loss rate D. The plasma gradient changes in times as

$$\frac{\partial \lambda}{\partial t} = S - D\lambda, \tag{5.2}$$

where S is the particle source and is kept constant in time. Equation (5.2) is deduced from the density continuity equation. The evolution equation for the loss rate D, The ratio of the dynamical flux to the gradient, is employed as

$$v\frac{\partial D}{\partial t} = D(\hat{\lambda}) - D \tag{5.3}$$

which indicates the temporal evolution of the radial electric field. Equation (5.3) corresponds to the normalized form of the equation of the poloidal motion. The nonlinear relation between the flux and gradient in the stationary state is expressed as $\hat{D}(\lambda) \equiv \hat{\Gamma}/\lambda$ and is given as in Fig.11(a). The variable t is normalized by ρ_{pi}^2/D_{e0}^b. The coefficient v in Ep. (5.3) is approximated as $v = (1+v_A^2/c^2)B_p^2/B^2 \simeq B_p^2/B^2$ where v_A is the alfvén velocity [43]. Therefore we take v as a smallness parameter. The smallness parameter v shows that Eq. (5.3) has a faster time scale than that of Eq. (5.2). Equation (5.3) is a sort of the time-dependent Ginzburg-Landau equation. This set of equations is used to study the dynamics associated with L/H transitions and spontaneous oscillaion, *i.e.*, ELMs, in the zero-dimensional model. Nonlinear oscillation solution for λ is obtained. The behavior of the particle outflux depends on the values of the source them S. The transition like $A \to E' \to B' \to C \to C' \to B \to B'$ occurs in the condition of $\hat{D}(B)\lambda(B) < S < \hat{D}(C)\lambda(C)$. The variables $\hat{D}(A)$ and $\lambda(A)$ represent the value of $\hat{D}$ and λ at the point denoted by the argument A in Fig.11(a), respectively. Figure 12 illustrates a typical example of the evolution for λ and loss flux Γ ($=D\lambda$) for the parameters of $S=0.16$ and $v=0.01$. Pulsative (periodic) solution for Γ is obtained. This result corresponds to dithering ELMs. On the other hand, the condition that the transition like $A \to E' \to B' \to C \to C' \to D \to D' \to E \to E'$ takes place is $\hat{D}(E)\lambda(E) < S < \hat{D}(E')\lambda(E)$. Figure 13 shows the time evolution for λ and loss flux Γ for the parameter of $S=0.05$ and $v=0.01$. Similar to the result in Fig.12, the periodic solution is obtained, however, the two different kinds of bursts are found to be put together. A new type of dithering ELMs is predicted theoretically and we name it 'compound dithers'.

5.4 Condition of the L/H transition which includes the double hysteresis

The condition of the L/H transition including the loss cone loss of ions and the anomalous loss is given as

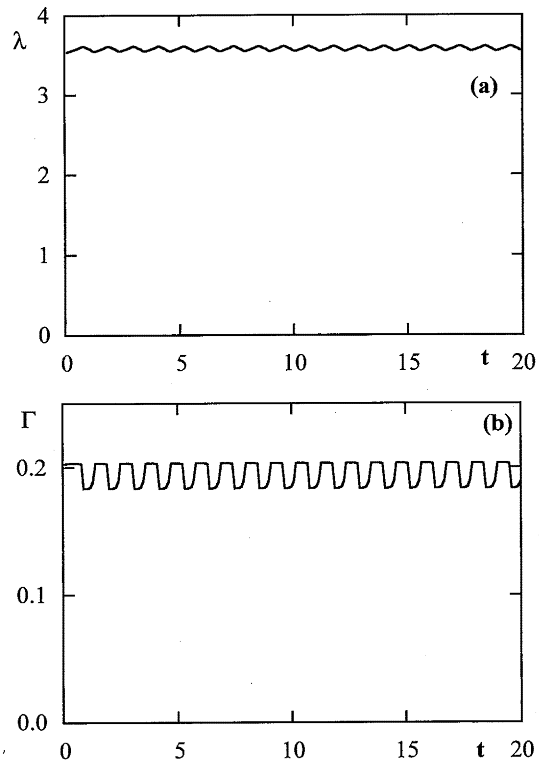

Fig. 12 Typical evolutions of (a) λ and (b) Γ. Parameters are as follows: $d=0.05$ and $S=0.16$. Self-generated oscillation like Fig.12 (b) corresponds to the dithering ELMs.

$$d=\frac{\sqrt{\nu_{*i}}\cdot\exp\{-\sqrt{\nu_{*i}}\}}{\lambda}. \tag{5.4}$$

in terms of the effective collisionality ν_{*i} and the gradient parameter λ. Similarly, the L/H transition condition when considered the bulk viscosity loss of ions in addition to the above bipolar losses is obtained as

$$d=\frac{2\left(\sqrt{\nu_{*i}}\cdot\exp\{-\sqrt{\nu_{*i}}\}+\Gamma_i^{bv}(\hat{U}_{p,m}=0,\lambda)\right)}{3\lambda}. \tag{5.5}$$

The critical λ where the L/H transition appears is given as the function of ν_{*i}. The results are shown in Fig.14(a)(b) according to Eqs. (5.4) and (5.5), respectively. The contour lines where the L/H transition occurs are given in $\lambda-\nu_{*i}$ plane for the various values of d. We can see that the critical λ value becomes higher when the parameter d is small (*e.g.,* $d=0.05$) in the case of including the bulk viscosity loss Γ_i^{bv} (Fig.14(b)) than in the case of neglecting it (Fig.14(a)). However, in the large d region (*e.g.,* $d=0.200$), the outstanding difference of the critical λ value can not seen comparing the both cases. In Fig. 14, the double hysteresis characteristics are indicated in the shaded parameter region.

6. Theoretical model of H-mode transition triggered by condensed neutrals near X-point

6.1 Introduction

The role of neutrals in L/H transition theory was discussed and it was predicted that H-mode confinement might be corrupt [9, 42]. The transfer of the momentum via collisions from transit ions to neutrals modifies E_r. It has been observed in experiments that a large neutral density prevents the H-mode transition [1]. Contrary to this conventional knowledge, however, it is observed that the H-ode is triggered by the neutrals injected by gas-puff near the X-point in

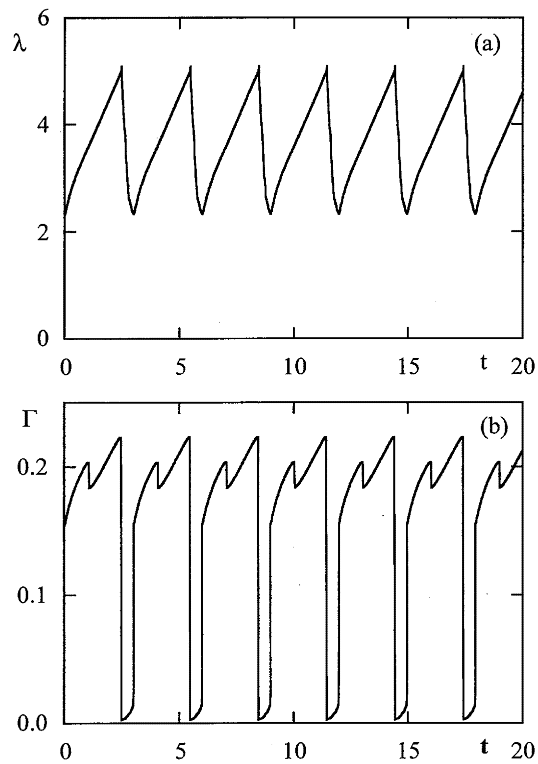

Fig. 13 Temporal traces for (a) λ and (b) Γ. Parameters are $d=0.05$ and $S=0.05$. Two hysteresis characteristics due to the bulk viscosity make the oscillation different from Fig.12. Two kinds of bursts are put together.

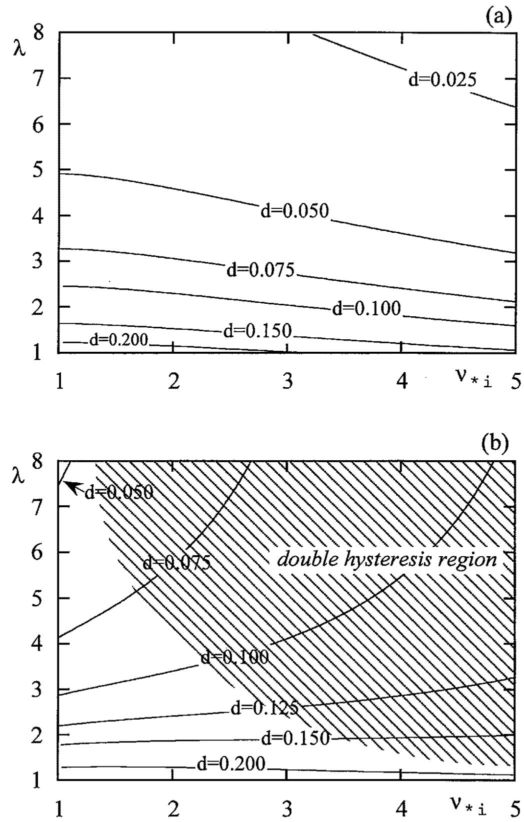

Fig. 14 Contour lines in $\lambda-\nu_{*i}$ plane as the L/H transitions. The case including the bulk viscosity loss corresponds to (b) and the case considering only the loss cone loss and the anomalous loss corresponds to (a).

JFT-2M [54].

In this chapter, we analyze the impact of neutral particles near X-point on the L/H transition, in order to address this experimental result [54]. As reviewed in Refs. [43, 44], theories on the H-mode phenomena have been developed from two aspects; *i.e.*, explanations of the L/H transition, and of the reduction of the anomalous transport. Here, the study is focused to the transition physics. The sudden change of the electric field, which is predicted to appear due to the neutrals near the X-point, is considered to cause the reduced transport as has been discussed in several theories [43, 44]. The model theory for the L/H transition is extended in the following. Four mechanisms for the electric field and electric field shear generation are simultaneously examined. The effects of the neutral density at the main plasma are included in the ambipolar condition as the ion loss via the collisions. The solutions of the loss flux are obtained as the function of the radial electric field and the plasma gradient. This solution has the hysteresis characteristic. The characteristic of the transition is examined to study the roles of neutral particles both at the main plasma and near X-point. It is found that the neutrals near the X-point cause the additional ion loss, and that this loss can trigger the L/H transition. The consistency between the prediction of the model theory and the experimental results is also discussed.

The constitution of this chapter is as follows. In Section 6.2, the stationary condition at the main plasma, which corresponds to the ambipolar condition is derived. For the typical parameter regime of JFT-2M, the loss rate is solved as the solutions of the ambipolar conditions. In Section 6.3, analysis on the H-mode transition condition is made. The contents of this chapter are reported in Ref. [55].

6.2 Stationary state

The equation in terms of the radial electric field is written as $(\varepsilon_\perp \varepsilon_0/e)\partial E_r/\partial t = \Gamma_{e-i}^{anom} - \Gamma_i^{lc} - \Gamma_i^{bv} - \Gamma_i^{n} \pm$ (*other losses*), where ε_0 is the dielectric constant of the vacuum and $\varepsilon_\perp$ is the perpendicular dielectric coefficient. This corresponds to the equation of the ion poloidal momentum.

We examine the ambipolar (stationary) condition at main plasma in tokamak. We consider the charge neutrality on the magnetic surface in the transport barrier. The ion loss cone loss is caused by the ion-ion collision near the main plasma or by the collision of ions with neutral particles in the X-point region. Therefore, the loss cone loss, Γ_i^{lc}, is the sum of the loss cone loss in both regions. The ion loss cone loss is given in the general form as

$$\Gamma_i^{lc} = \frac{n_i \nu_{eff} \sqrt{\varepsilon \rho_{pi}}}{[\nu_{*i} + X^4]^{\frac{1}{2}}} \exp\{-[\nu_{*i} + X^4]^{\frac{1}{2}}\}. \tag{6.1}$$

The effective detrapping frequency ν_{eff} is defined as $\nu_{eff} = \nu_{ii} + \nu_{in_0^X}$, where ν_{ii} is the ion-ion collision frequency and $\nu_{in_0^X}$ is the collision frequency of trapped ions with the neutral particles near the X-point. It is assumed that the collision between ions and neutral particles near the X-point does not affect the banana orbit of ions. In addition to Γ_i^{lc}, the loss due to the collisions between transit ions and neutrals (Γ_i^n), the loss due to the bulk viscosity (Γ_i^{bv}) and the bipolar component of the anomalous loss (Γ_{e-i}^{anom}) are taken into account.

We consider the thin region enclosed by two magnetic surfaces inside the separatrix, where the transport barrier is to be formed. (see Fig.15) The ion orbit may deviate from this tube, however, we assume the loss cone loss from this region. An additional loss cone loss due to neutral-ion collision near the X-point is contributed from banana ions passing through this shaded region. We assume that the electric field is uniform along the magnetic surface and that the electric field at the main plasma and near the X-point take the same value. In other word, the same value of the electric field is used as the averaged value over the shaded portion. Imposing the stationary condition at main plasma near the midplane, *i.e.*, $\Gamma_i^{lc} + \Gamma_i^{bv} + \Gamma_i^n = \Gamma_{e-i}^{anom}$ and using the models of the bipolar losses, we obtain the equation to determine the relation between the flux and the plasma gradient as

$$\frac{\nu_{*i} + \xi}{[\nu_{*i} + X^4]^{\frac{1}{2}}} \exp\{-[\nu_{*i} + X^4]^{\frac{1}{2}}\} + \frac{\sqrt{\pi}}{4}$$

$$(I_p \cdot X + 0.2 I_t) + d_n(\lambda_i + X) = d(\lambda - X) (\equiv \hat{\Gamma}), \tag{6.2}$$

where $d_n = n_0^{main} \langle \sigma v \rangle (1 + 2q^2)/(\sqrt{\varepsilon}\omega_b q^2)$ and n_0^{main} is the neutral density at the midplane. A parameter ξ represents the effect of the neutral density near X-point, which is defined as $\xi=\nu_{in_0^X}/\omega_b$. The parameter d stands for the ratio of the mobility of electrons to ions. The thermodynamic forces: $\lambda_i=-\rho_{pi}(n'_i/n_i+\alpha_i T'_i/T_i)$, $\lambda=-\rho_{pi}(n'_e/n_e+\alpha T'_e/T_i)$, where the density and the temperature of ions are estimated at the main plasma. Equation (6.2) is derived with the assumptions: $n_i=n_e(\equiv n)$, $T_i=T_e(\equiv T)$ and $U_{p,m}=X$. The parameters used in the following calculations are similar to those of JFT-2M tokamak as shown in Section 5.2. We fix $d=0.72$ and $\nu_{*i}=2.0$. In this parameter regime of JFT-2M tokamak, the values of the density and the temperature in the shaded portion in Fig.15 are estimated as about $n=1.0\times10^{19}(m^{-3})$ and $T=100(eV)$, respectively. For simplicity, we set $\lambda=\lambda_i$ and $U_{p0}B/(v_{Ti}B_p)=0.2$. The neutral density n_0^{main} at the main plasma is evaluated as $n_0^{main}=5.0\times10^{17}\cdot d_n\cdot T_{100}^{1/6}(m^{-3})$, ($T_{100}$ in unit of $100(eV)$) when the neutral-ion collision at the main plasma is considered to induce the charge-exchange. If the collision between banana ions and neutral particles near the X-point is also assumed to induce the charge-exchange, the neutral density n_0^X can be evaluated as $n_0^X=1.5\times10^{18}\cdot\xi\cdot T_{100}^{1/6}(m^{-3})$, where n_0^X is the neutral density near the X-point. The ratio n_0^X/n_0^{main} is estimated as 3.0 $\cdot\xi/d_n$ for the set of parameters used here.

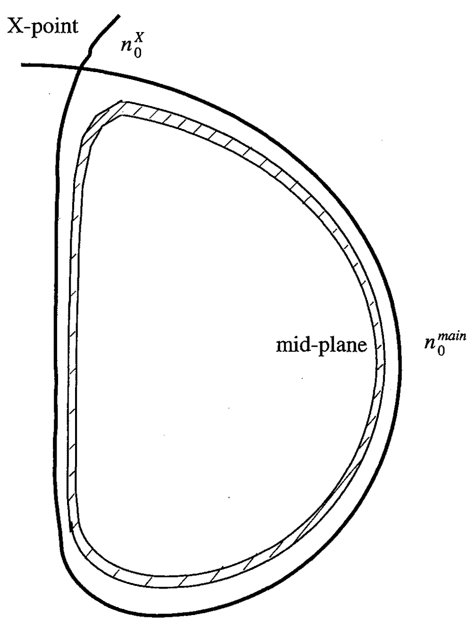

Fig. 15 The thin magnetic surface tube inside the separatrix, where the transport barrier is formed. The parameters n_0^{main} and n_0^X represent the neutral density at the main plasma and near the X-point, respectively.

We investigate the cases of the various values of d_n for the fixed value of $\xi=0.5$, in order to examine the effects of the neutral at the main plasma on the L/H transition. Figure 16 shows the solutions of Eq. (6.2). The variations of the normalized radial electric field X (a) and the normalized particle flux $\hat{\Gamma}$ (b) as the functions of the normalized gradient parameter λ are plotted. In the present parameter regime, the loss due to the collisions between transit ions and neutral particles makes the L/H transition softer than the case only with the loss cone loss of ions and the anomalous loss. Furthermore, the jump of the flux at the L/H transition is smaller (shallower transition) when the loss due to the collisions between transit ions and neutrals exists. As seen from Fig.16, the jump at the L/H transition decreases and finally disappears as d_n increases. This prediction is qualitatively in agreement with the experimental results that the neutrals at the main plasma prevent the H-mode transition [1]. In this parameter region, the jump of the radial electric field X at the L/H transition is predicted to occur from the negative E'_r to the positive E'_r. When λ becomes large, the loss due to the collisions between transit ions and neutral particles is dominant compared to the loss cone loss of ions. In this case, $\Gamma_i^{lc}:\Gamma_i^{bv}:\Gamma_i^{n}=10:1:50$ for $\lambda=2$ and $d_n=0.5$. Especially, the loss due to the collisions between transit ions and neutral particles is considerably large in the case $d_n=0.5$ since $\hat{\Gamma}_i^n$ is proportional to the value of the neutral density at the main plasma. ($\hat{\Gamma}_i^n$ is the third term in the left hand in Eq. (6.2).) The value $d_n=0.5$ corresponds to the case of $n_0^{main}/n=2.5\times10^{-2}$ for $n=1.0\times10^{1}(m^{-3})$ in the standard parameter region.

In order to investigate the effect of the neutral particles near the X-point on the L/H transition, we next examine the cases for the various values of ξ for the fixed value of $d_n=0.4$. The case $\xi=1.0$ corresponds to $n_0^X=1.5\times10^{18}(m^{-3})$ and $n_0^X/n=0.15$. In the case of $\xi=2.0$ and $d_n=0.4$, the ratio $n_0^X/n_0^{main}=1.5\times10$. Figure 17 shows X (a) and $\hat{\Gamma}$ (b) v.s. λ as the solutions of Eq. (6.2) where the value of ξ is varied. Similar to the results in Fig.16 (a), it is predicted that the jump of the radial electric field X at L/H transition occurs from the negative E'_r to positive E'_r. It is demonstrated that the large flux jump at the

L/H transition is obtained, especially in the case of the higher density of neutrals near the X-point: $\xi=2.0$. It should be essential that neutrals are localized in the region of X-point and divertor plate and that the neutrals in the core are suppressed. This prediction agrees with the experimental results in the higher density regime of neutrals near the X-point. The softer transition is obtained in the case of lower neutral density: $\xi=1.0$. This change from the L-mode branch of the large flux to the H-mode branch of the low flux occurs gradually in $\hat{\Gamma}-\lambda$ plane. This variation may be seen as the gradual improvement of the confinement with heating. Note that the confinement quality of the obtained H-mode is shown to be low. The presence of the neutrals near the X-point

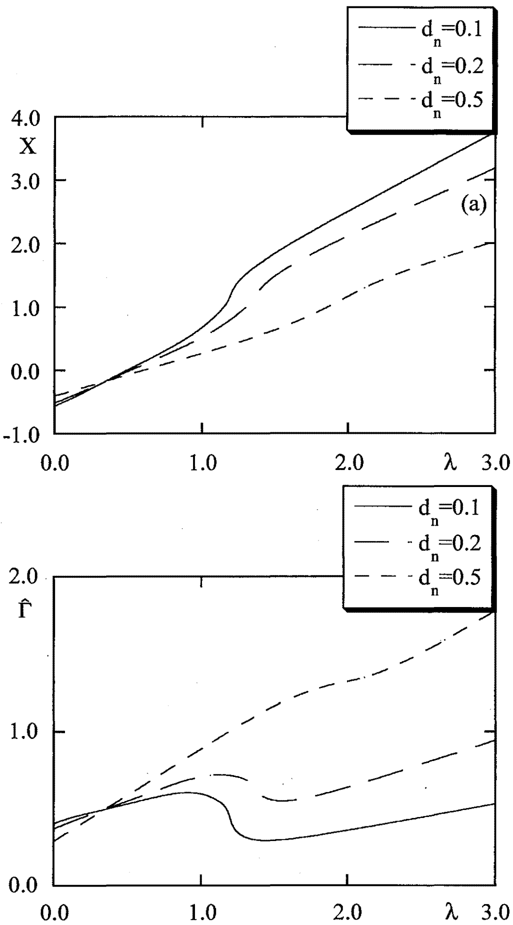

Fig. 16 Solutions for (a) the radial electric field and (b) the normalized particle flux as the functions of λ. (for the case of $d=0.72$, $\nu_{*i}=2$ and $\xi\ (\equiv \nu_{in_0}^{X}/\omega_b)=0.5$) The change in the L/H transition due to the neutral particles at the main plasma is shown.

does not affect the H-mode confinement and makes the L-mode confinement worse in this model. These are seen in Fig.17 since the flux $\hat{\Gamma}$ increases in the region $0.0<\lambda<2.5$ and does not change in the region $\lambda>2.5$. In the case of $\xi=1.0$, the jump of the flux in the L/H transition is found to be small and is about a half of the case with $\xi=2.0$. If ξ becomes smaller, $\hat{\Gamma}$ becomes a monotonically increasing function of the gradient λ. The hard transition associated with the multiple solutions disappears. This implies that the lower limit of the neutral density near the X-point exists to realize the L/H transition. When the neutral particles near the X-point do not exist, *i.e.,* for the case of $\xi=0.0$, the L/H transition does not occur this case.

The critical neutral density near the X-point alters if the values of ν_{*i} and dn are changed. We here show their dependences in the following. For simplicity, we neglect the contribution of the bulk viscosity loss. It is found that a multiple solution exists if ξ is above the value ξ^*:

$$\xi^*=\frac{(d+d_n)\left(\dfrac{1}{2}+\sqrt{\nu_{*i}}\right)^3\exp\left(\dfrac{1}{2}+\sqrt{\nu_{*i}}\right)}{2\left(\dfrac{1}{4}+\sqrt{\nu_{*i}}\right)^{\frac{3}{4}}\left(\dfrac{3}{2}+\sqrt{\nu_{*i}}\right)}. \tag{6.3}$$

If ξ becomes small and the condition

$$\xi<\frac{d_n\left(\dfrac{1}{2}+\sqrt{\nu_{*i}}\right)^3\exp\left(\dfrac{1}{2}\sqrt{\nu_{*i}}\right)}{2\left(\dfrac{1}{4}+\sqrt{\nu_{*i}}\right)^{\frac{3}{4}}\left(\dfrac{3}{2}+\sqrt{\nu_{*i}}\right)}(\equiv\xi^c) \tag{6.4}$$

is satisfied, $\hat{\Gamma}$ becomes a increasing function of λ as seen in the case of $d_n=0.5$ in Fig.17 (b). In the region $\xi^c<\xi<\xi^*$, a negative slope of $\hat{\Gamma}$ appears and a soft transition is predicted. The parameter ξ^c stands for the lower limit of neutral density near the X-point to realize the L/H transition. The critical neutral density ξ^c near the X-point is shown in Fig.18 as the functions of ν_{*i} and d_n. It is obtained that the value of ξ^c becomes large when the collisionality ν_{*i} and the neutral density at the main plasma d_n increase. This implies that a large neutral density near the X-point for the H-mode transition is needed when the values of ν_{*i} or d_n are large. In the case of $d_n=0.1$, the change of ξ^c remains to be about 2.0 for $1\leq\nu_{*i}\leq5$. However, in the case of $d_n=0.5$, the change of ξ^c

becomes larger and is more than 10.0.

6.3 Condition for the L/H transition

The critical pressure gradient λ also alters if the values of parameters ν_{*i} and d are changed. The condition of L/H transition is estimated as

$$d-d_n=\frac{(\nu_{*i}+\xi)\cdot\exp\{-\sqrt{\nu_{*i}}\}/\sqrt{\nu_{*i}}+\hat{\Gamma}_i^{bv}(X=0)}{\lambda}. \tag{6.5}$$

The critical λ where L to H transition occurs is parametrically surveyed with respect to ν_{*i}. The result is shown in Fig.19. The traces of the point where L/H transition occurs are shown in $\lambda-\nu_{*i}$ plane for the various value of d, where ξ is fixed to 1.0. We see that, in the smaller d region $(d-d_n=$ 0.075, 0.100), the higher the collisionality ν_{*i} is, the higher the critical λ value becomes. However, in the large d region $(d-d_n=0.125\sim 0.250)$, the change in the critical λ becomes small and remains to be order of $\triangle\lambda=0.5$ for $1\leq\nu_{*i}\leq 5$. When the value of d becomes smaller, the transition characteristic becomes harder ever in the presence of the neutral particles [9]. The example is shown in Fig.20, where the parameters are $\nu_{*i}=2.0$, $d_n=0.1$ and $\xi=2.0$. In the case of $d=0.2$, the hysteresis is obtained. This is due to the cusp-type nature of the transition. In such a case, a larger amount of neutral particles at the main plasma needs to kill the L/H transition.

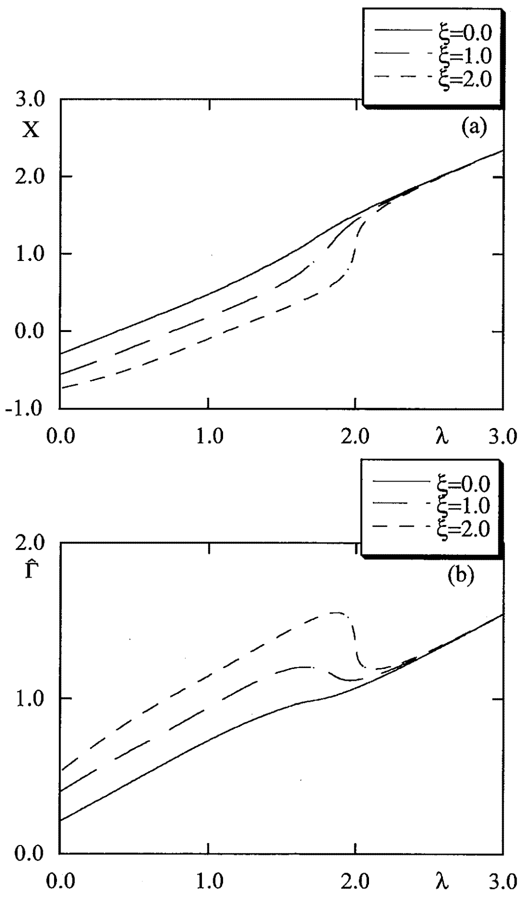

Fig. 17 The variation of the L/H transition for the various values of the neutral density near X-point. Solutions for (a) the radial electric field and (b) the normalized particle flux as the functions of λ are shown. he parameter d_n is set to $d_n=0.4$. The parameters are same as those in Fig.16.

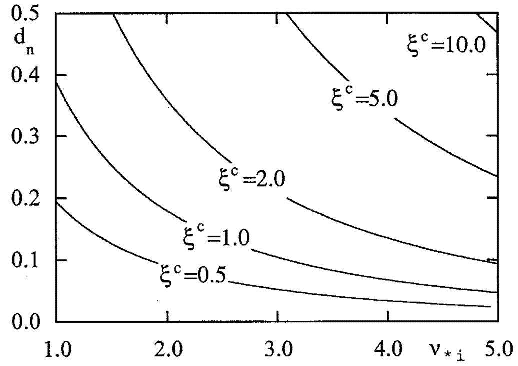

Fig. 18 The contour line of ξ_c on the d_n-ν_{*i} plane. The parameter ξ_c stands for the lower limit of the neutral density near the X-point for the L/H transition. We set $\Gamma_i^{bv}=0$, for simplicity.

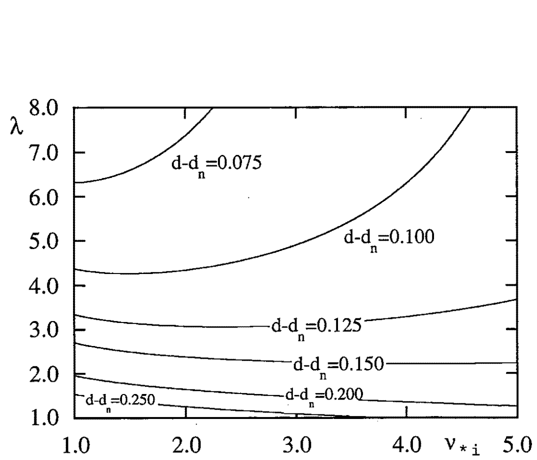

Fig. 19 The contour line of d as the L/H transition condition on the λ-ν_{*i} plane. The parameter ξ_c is set to $\xi=1.0$.

7. Change of H-mode dynamics due to edge electric field shear

7.1 Introduction

In this chapter, the model theory [27] for the dithering ELMs is extended. The effects of E'_r are included in the models of the bipolar losses. Using the extended model for the dithering ELMs as the cyclic oscillation between L- and H-phases, the characteristic of the self-generated oscillation is studied further. Assuming the ambipolar condition, the solution of the loss flux is obtained as the functions of the radial electric field, the radial electric field shear and the plasma thermodynamic force. This solution has the hysteresis characteristics. Introducing an approximate relation between the electric field and electric field shear, three variables are contracted into two. Using the loss flux so-defined, the local transport model is shown. The existence of a limit cycle solution is confirmed in the presence of the radial electric field shear as well as of the radial electric field. The region for the occurrence of the self-generated oscillation, considering the effects of electric field shear, is also obtained in the parameter range of d (the relative electron loss rate to the loss cone loss rate). The radial electric field shear is found to affect this range.

The constitution of this chapter is as follows. In Section 7.2, the stationary condition, which corresponds to the ambipolar condition, using the models of bipolar losses, is derived. In Section 7.3, coupled dynamic equations for the plasma gradient and the loss rate are solved. In Section 7.4, the condition for the self-generated oscillation is presented. The contents of this chapter are reported in Ref. [56].

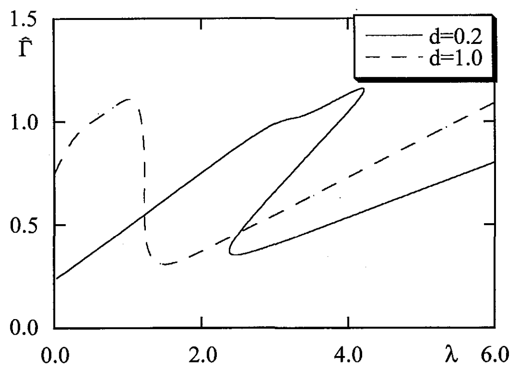

Fig. 20 The change of the characteristic of the L/H transition due to the parameter d is shown. As the parameter d becomes small, the hysteresis appears. The other parameters are d_n=0.1, ξ=2.0, and ν_{*i}=2.0.

7.2 Stationary condition

The equation in terms of the radial electric field is written as $(\varepsilon_0\varepsilon_\perp\partial E_r/\partial t)/e=\Gamma_{e-i}^{anom}-\Gamma_i^{lc}\pm$ (*other losses*). This corresponds to the equation of the ion poloidal momentum. Imposing the stationary condition, *i.e.*, $\Gamma_i^{lc}=\Gamma_{e-i}^{anom}$, we have the equation to determine the relation between the ambipolar electric field and its shear for given λ_r as

$$d_0(\lambda_r-X)\sqrt{1+\frac{u_g}{u_c}}=\frac{\exp(-X^2)}{\sqrt{|1-u_g|+C\varepsilon}}, \tag{7.1}$$

using Eqs. (3.6) and (3.8). Here, $\lambda_r=-\rho_{pi}(n'_e/n_e+\alpha T'_e/T_e+eBr\omega/(MT\mathrm{e}))=\lambda-\rho_{pi}(eBr\omega/(MT\mathrm{e}))$ and $d_0=D_{e0}^b\sqrt{\varepsilon}/(\hat{F}\nu_{ii}\rho_{pi}^2)$. For simplicity, we set $n_i=n_e$ $(\equiv n)$ and $T_i=T_e(\equiv T)$ in deriving Eq. (7.1).

The solution (X, u_g) exists for various values of the thermodynamic force λ_r. The variable X relates u_g with λ_r through the force balance. The radial force balance equation requires

$$E_r=\frac{\nabla p_i}{en_i}-u_pB_t+u_tB_p, \tag{7.2}$$

where u denotes the plasma fluid velocity, p_i is the pressure of ions and the subscripts p and t stand for poloidal and toroidal components, respectively. Furthermore, the poloidal bulk viscosity leads the relation $u_p/u_{Ti}\propto\varepsilon\rho_{pi}\nabla T_i/(qTi)$ [57]. This relation gives $X=-\lambda_i-u_t/v_{Ti}$, where $\lambda_i=\rho_{pi}(n'_i/n_i+\alpha_iT'_i/T_i)$ and α_i is a numerical coefficient of the order of the unity. As the toroidal flow in the scrape-off layer is damped due to the parallel loss along the field line, u_t is much smaller than v_{Ti} near the edge [58]. Next we use simple assumptions: $\omega=0$ and $\lambda=\lambda_i$. So we obtain the relation $X=-\lambda$. Substituting $X=-\lambda$ into Eq. (7.1), we obtain the equation for the stationary solutions,

$$2d_0\lambda\sqrt{1+\frac{u_g}{u_c}}=\frac{\exp(-\lambda^2)}{\sqrt{|1-u_g|+C\varepsilon}}\left(\equiv\hat{\Gamma}(u_g,\lambda)\right), \tag{7.3}$$

in terms of u_g and λ, where the symbol denotes the stationary variable. Having solved Eq. (7.3), the hysteresis curves of u_g, $\hat{D}$ ($\equiv \hat{\Gamma}/\lambda$) and the particle flux have been obtained as functions of the gradient parameter λ [20]. Figure 21 shows a typical stationary solution of Eq. (7.3) in terms of $\hat{D}$ as the function of u_g and λ, where the constant-ℓ approximation, *i.e.*, $E'_r=E_r/\ell$, is employed. Parameters are chosen as $d_0=0.5$, $C=2.0$ and $\varepsilon=0.3$, where $u_c=2.76$. The trajectory of the solution clearly shows the nature of the cusp-type catastrophe. The projection of the curve of $\hat{D}$ (u_g, λ) onto $\hat{D}-\lambda$ plane is shown in Fig.22. When we consider the case of $u_g \rightarrow 0$, with the constraint of $E_r \neq 0$ (*i.e.*, $\ell \rightarrow \infty$), we recover the original hysteresis model proposed in Ref. [8]. We see that the shape of the curve in Fig.22 changes depending upon a constraint for the relation between E'_r and E_r. However, the generic nature of the cusp is not altered. The relation to the shape of the burst will be discussed later.

7.3 Temporal evolution and self-generated oscillation

In this section, we investigate the dynamics of the H/L transition and obtain the self-generated oscillation near the transition boundary. Similar to Section 5.3, we choose two dynamical variables, *i.e.*, the gradient parameter λ and the dynamic loss late D which is considered to be the function of E_r and E'_r. The plasma gradient, λ, changes in time as

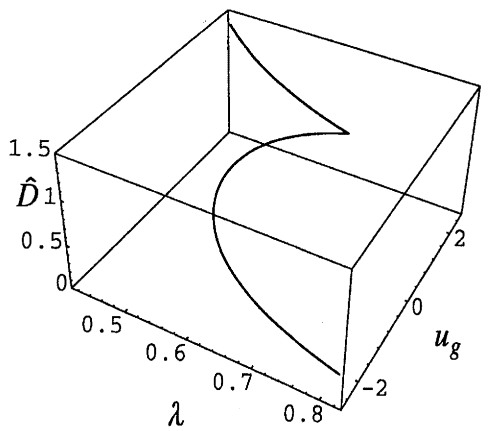

Fig. 21 The solutions of Eq. (7.3) in the $\hat{D}$ (λ, u_g) space are sketched. The bird-eye view of the hysteresis curve for the diffusion coefficient $\hat{D}$ v.s. λ and u_g is shown. The constant-ℓ approximation is employed to deduce it. The parameters are $d_0=0.5$, $C=2.0$, $u_c=2.76$ and $\varepsilon=0.3$.

$$\frac{\partial \lambda}{\partial t}=S-D\lambda, \tag{7.4}$$

where S is the particle source and is kept constant in time. Equation (7.4) is deduced from the continuity equation of the density. The equation for the dynamic loss late D, the ratio of the dynamical flux to the gradient is given by,

$$v\frac{\partial D}{\partial t}=\hat{D}(\lambda)-D, \tag{7.5}$$

which is deduced from the equation of the ion poloidal momentum which describes the temporal evolution of the radial electric field. This set of Eqs. (7.4) and (7.5) corresponds to an extended version of the previous analysis [27, 28]. The effect of the radial electric shear are added to Eq. (7.5). The variable t is also normalized by ρ_{pi}^2/D_{e0}^b. The parameter v indicates a small parameter $O(B_p^2/B_t^2)$. The nonlinear relation between the loss rate and the gradient in the stationary state is shown in Fig.22. Using the 0-D transport equations, *i.e.*, Eqs. (7.4) and (7.5), we confirm the existence of a self-generated oscillation with the E'_r contribution. We examine the time evolution of the particle outflux Γ at the plasma edge near the transition boundary of the L and H phases. In Fig.23, the typical temporal evolution of λ and Γ are shown. Under the constant supply of the particle flux Γ_{in}, $\Gamma_{in}\equiv S$ for fixed d_0, we obtain the self generated oscillations of λ and Γ. The large amplitude oscillation of Γ corresponds to H_α burst and the oscillation of λ with a small amplitude is seen. The parameters are $S=0.62$ and $v=0.01$. The self-generated oscilla-

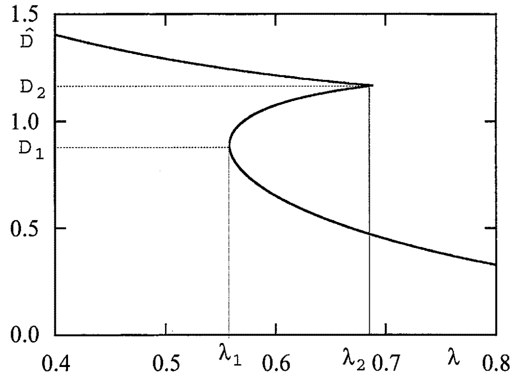

Fig. 22 The projection of the solution $\hat{D}$ (λ, u_g) in Fig.21 onto $\hat{D}-\lambda$ plane.

tion which explains the dithering ELMs was predicted in the presence of only E_r [27]. The outflux Γ which is obtained here oscillates between L and H mode in the space of Γ (u_g, λ). The same characteristic is found to remain with an inclusion of E'_r. The period of the self-generated oscillation in this case is predicted to be about 1.0 (msec) for the parameters of $D^b_{e0}=0.5\,(m^2/s)$, $T_i=100\,(eV)$, the toroidal magnetic field $B_t=1.3\,(T)$ and $q=3$. This value is almost the same extent as the period in the experiment [21]. Note that the form of the bursts shown in Fig.23 is strongly affected by the nature of the cusp structure, for example, the ridge points and the shape near the ridge points of the curve in Fig.22. The cusp structure changes depending on the value of d_0 (including n_i, T_i and D^b_{e0}). The values of the plasma gradient parameter λ and the loss rate $\hat{D}$ at the transition points will be analyzed in the next section. The shape of the burst is also affected by the influx Γ_{in}, in other words, the source term S. The variety of evolutions of Γ other than that shown in Fig.23 is predicted.

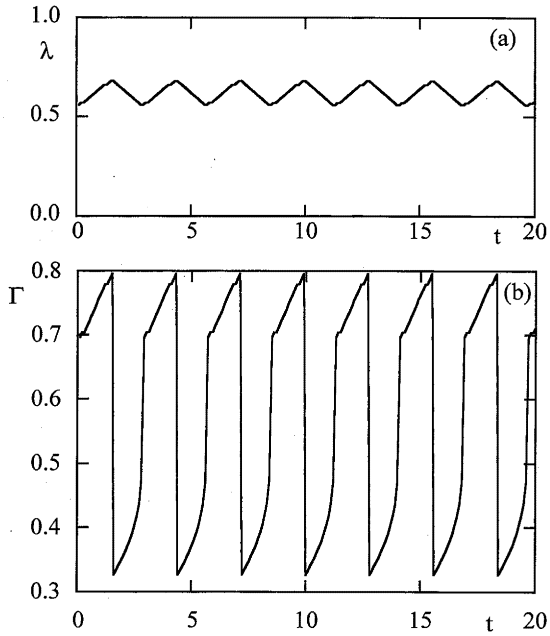

Fig. 23 Temporal evolutions of the plasma gradient λ (a) and the outflux Γ (b) at the edge. Parameters are $S=0.62$, $v=0.01$ and $d_0=0.5$. The self-generated oscillation is also confirmed in the presence of E'_r, similar to when considering only E_r.

7.4 Condition for self-generated oscillaion

Let us examine the condition for the occurrence of the self-generated oscillation obtained in Section 7.3. The $\hat{D}-\lambda$ curve which is shown in Fig.22 governs the characteristics of oscillations. At the ridge points of (λ_1, D_1), the $H\rightarrow L$ transition occurs and (λ_2, D_2) is the point at which the $L\rightarrow H$ transition occurs. When the electric field shear is not taken into account, the values of λ_1, λ_2, D_1 and D_2 were estimated and given in Ref. [27]. In order to extend the results in Ref. [27], the values of the ridge points are estimated, analyzing the solution of Eq. (7.3). We have the approximate relations with inclusion of the electric field shear as,

$$\lambda_1=\sqrt{\ln\frac{2e}{d_0\sqrt{1+C\varepsilon}}}\,, \tag{7.6}$$

$$\lambda_2=\frac{1}{d_0\sqrt{C\varepsilon(1+\zeta)}}, \tag{7.7}$$

$$D_1=\frac{d_0}{2\ln\dfrac{2e}{d_0\sqrt{1+C\varepsilon}}}, \tag{7.8}$$

$$D_2=d_0\sqrt{1+\zeta}\left[1-\frac{1}{2}(1+\zeta)C\varepsilon d_0^2\right], \tag{7.9}$$

where

$$\zeta=\frac{u_g}{u_c} \tag{7.10}$$

denotes the effect of E'_r on (λ_1, λ_2, D_1, D_2).

The stability analysis of the nonlinear curve, Eq. (7.3), gives the characteristics of the solution. If $D_1\lambda_1>D_2\lambda_2$, the three solutions are stable. If $D_1\lambda_1<D_2\lambda_2$ holds, the solution in the middle becomes unstable. The condition for the occurrence of the self-generated oscillation on $\hat{D}-\lambda$ plane is given by

$$D_1\lambda_1<D_2\lambda_2, \tag{7.11}$$

Furthermore, for the appropriate value of influx Γ_{in}, the self-generated oscillation between L- and H-modes occurs. For example, the value of Γ_{in} ($=S$ for the fixed value of d_0) should satisfy the relation, $D_1\lambda_1<\Gamma_{in}<D_2\lambda_2$, for its occurrence. For other values of Γ_{in}, we only find the stationary L or H mode. Which type of the dynamic behavior occurs is determined by the value of Γ_{in}. If $D_1\lambda_1>D_2\lambda_2$ holds, any oscillations are not allowed. In such a case, the hard and direct transition from L-phase to H-phase (or vice verse) occurs. The detailed analyses but only in the presence of E_r were reported in Ref. [28]. Substituting Eqs. (7.6)-(7.9) into an inequality (7.11), the condition for self-generated oscillation for the given value of λ ($X=-\lambda$) is obtained as

$$\frac{\sqrt{(1+C\varepsilon)+8e^2(C\varepsilon)(1+\zeta)^2}-\sqrt{1+C\varepsilon}}{8e(C\varepsilon)(1+\zeta)^2}<d_0<1. \tag{7.12}$$

The terms of ζ in Eqs. (7.6)-(7.9) and in an inequality (7.12) represent the effect of the electric field shear E'_r. When we set $g_1=\lambda_1/n_L$, $g_2=\lambda_2/n_L$ (n_L is the typical value of λ in the L-mode.) and $\zeta=0$, Eqs. (7.6)-(7.9) recover the results in Ref. [27]. For the case of $\zeta=0$, the inequality (7.12) also reduces to $0.37<d_0<1.0$ [27] when the parameters are $C=2$ and $\varepsilon=0.3$. For the $E_r-E'_r$ model, we obtain the diagram of the occurrence region of the self-generated oscillation on $d_0-\zeta$ plane. The result is shown in Fig.24 when the parameters are chosen to be $C=2$ and $\varepsilon=0.3$. The wider region is predicted for the negative $E'_r(u_g<0)$ than the positive E'_r.

7.5 Chaotic characteristics for the self-generated oscillation

Near the L/H transition points in the hysteresis curves shown in Fig.21 and Fig.22, the self-generated oscillation exists under a certain condition in Section 7.4 or Ref. [27]. Model of the development equation

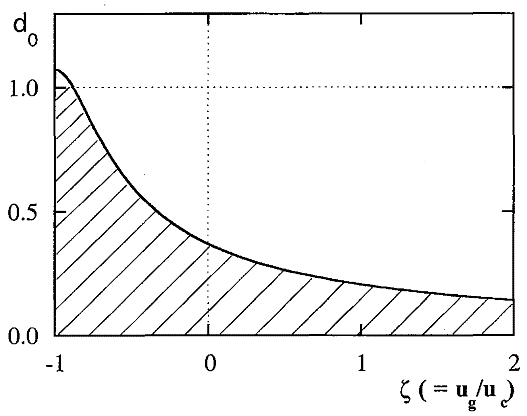

Fig. 24 Parameter space on $d_0-\zeta$ plane for the self-generated oscillation in the presence of E'_r(hatched region), where $\zeta=u_g/u_c$. The parameters are $C=2.0$ and $\varepsilon=0.3$.

of the thermodynamic force for the 0-D analysis is given as

$$\frac{\partial\lambda}{\partial t}=S-D\lambda, \tag{7.13}$$

where λ is the gradient parameter, S is the source and D is the effective diffusivity. The effective diffusivity D is the multivalued function of λ and is modeled as

$$v\frac{\partial D}{\partial t}\frac{1}{D_L^2}=\frac{\lambda}{\lambda_L}-1-\beta\left(\frac{D}{D_L}-1\right)^3+\beta_2\left(\frac{D}{D_L}-1\right), \tag{7.14}$$

where β_1 and β_2 are introduced for the dictation of the sharpness at the ridge points in the transition curve. For the simplicity of the argument, in the following the normalizations are made as $\lambda/\lambda_L\to\lambda$, $tD_L\to t$, $S/(\lambda_L D_L)\to S$ and $D/D_L\to D$. The normalizing value λ_L and effective diffusivity D_L correspond to those in the typical values of L-mode. Here, D_L^{-1} is the characteristic diffusion time in the layer of our interest in the L-mode, *i.e.*, ρ_{pi}^2/D_{e0}^b. Equation (7.14) is rewritten as

$$v\frac{\partial D}{\partial t}=\lambda-1-\beta_1(D-1)^3+\beta_2(D-1) \tag{7.15}$$

This set of equations is used to study the dynamics associated with L/H transition and spontaneous oscillation, *i.e.* a self-generated oscillation, not considering the electric field shear. The model of the source term S is given as $S=S_0+\varepsilon_f\sin(2\pi\Omega t)$, where parameters S_0, ε_f and Ω are constant in time. We first take the case that the external oscillation frequency is the original frequency, *i.e.*, $\Omega=1$. In this case, we find the mode locking and period doubling. Typical time traces are shown in Fig.25. In the case where the oscillation frequency Ω is much smaller than the intrinsic frequency, intermittent burst of loss is observed as shown in Fig.26. Some calculations are reported in Ref. [45].

8. Summary and discussion

In this article, we studied theoretical model of the H-mode transition in tokamaks based on the bifurcation of E_r and E'_r at the edge region. In Chapter 2, we surveyed the experimental results for the L/H transition and ELMs and reviewed the model theories with respect to the L/H transition physics. Next, in Chapter 3, we listed the models for bipolar losses, which were used in the latter chapters, in the presence of the radial electric field and its shear. In Chapters 4, 5, 6, 7, the model torques in the poloidal momentum balance were analyzed and the various types of the L/H transitions were examined. We introduce a constant-ℓ approximation in these analysis to study the point model for dynamics.

First of all, in Chapter 4, we extended the previous bifurcation model with the loss cone loss of ions and the anomalous loss of electrons to include the ripple loss of hot ions. Using the extended bifurcation model (Eq. (4.1)), we discussed the characteristics of the L/H transition in the typical parameter regime of JT-60U with various values of the temperature of hot ions (in Fig.9) and the bulk density (in Fig.10). The ripple loss of hot ions is found to make the L/H transition be softer and shallower. Especially, for the high density, the hard transition is predicted and does not contradict to the existence of ELMy-state in experiments. The soft transition (without the hysteresis characteristic) is obtained in a low density regime. This soft transition may explain the under L/H transition observed in JT-60U. When λ becomes large, the ripple loss is more noticeable than the loss cone loss of ions.

In Chapter 5, the dynamics of the L/H transition is studied by keeping three independent mechanisms of the bipolar losses, *i.e.*, the loss cone loss, ion loss by collisional bulk viscosity and anomalous bipolar loss. Zero-dimensional model is introduced and the

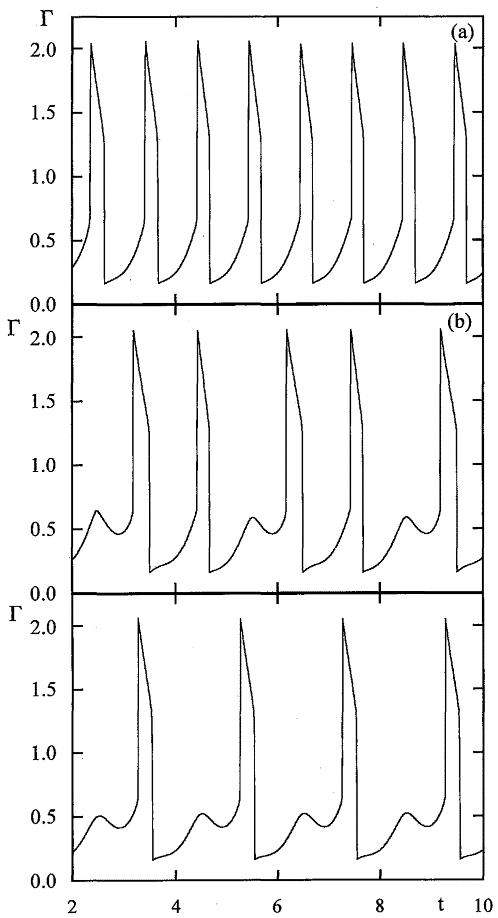

Fig. 25 Typical time evolution for the mode locked oscillation. Mode locking to the-fundamental oscillation (a) and to the subharmonics (b: 2/3 period and c: 1/3 period). Parameters are ε_f=0.25, Ω=1, S_0=0.68(a), 0.64(b), 0.505(c).

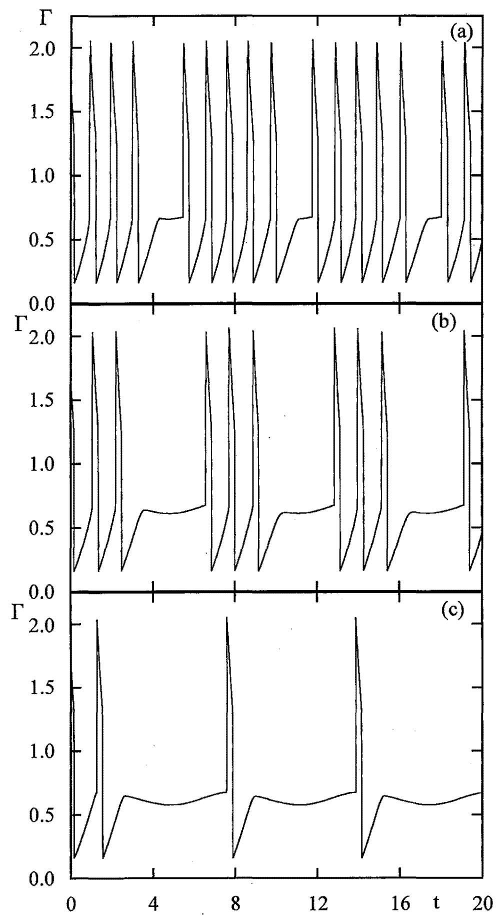

Fig. 26 Example of the time trace in the presence of low frequency external oscillation. Intermittency of the bursts is observed. Parameters are ε_f =0.05, Ω=1/(2π), S_0=0.71(a), 0.66 (b), 0.625(c).

bifurcation condition is analyzed. It is found that there can be a multiple bifurcations and five-fold multiple states in the gradient-flux relation. The double hysteresis characteristic is predicted. It is the case when the effective ion collisionality is of the order unity and these three terms have similar magnitude. The coupled temporal evolution of the plasma parameter and effective diffusivity is analyzed and the limit cycle solution with double hysteresis is newly found. This predicts the existence of a new type of ELMs and we attribute it to the compound dithers in experiments. The condition of the compound dithers, $d=0.05$ and $\nu_{*i}\sim 1$ critically depends on the assumption of the constant-ℓ model.

In Chapter 6, the role of neutral particles near the X-point and at the main plasma is studied by keeping four independent mechanisms of the bipolar losses, *i.e.*, the loss cone loss, the bulk viscosity loss, the ion loss due to the collision between the transit ions and the neutral particles and the anomalous bipolar loss. The 0-D model was employed and a simplication as $E'_r=E_r/\ell$ was done. The typical parameter ℓ was further assumed as a constant. Therefore, E'_r was assumed to have the linear relation to E_r. Ambipolar (Stationary) condition is examined at main plasma. The stationary solution of Eq. (6.2) of the high particle flux corresponds to the L-phase and that of the low flux corresponds to the H-phase, respectively. It is demonstrated that the neutral particles near the X-point can drive the H-ode transition. We first examined the roles of the neutral particles at the main plasma in the L/H transition. When the neutral density at the main plasma is increased, the flux change at the transition is increased, thus, the improvement of the confinement is predicted to be corrupt. If the neutral density at the main plasma is larger than the critical neutral density, the H-mode transition would not occur. The critical neutral density depends on the experimental precision. The quantitative agreement between the experiment and the theory can therefore be improved by including the effect of the ion loss due to the collision with the neutral particles at the main plasma in the model theory. Next the variety of the transition characteristic with the change of the neutral density near the X-point is obtained. It is shown that, for the given set of parameters, there exists a critical value of the neutral density near X-point above which the H-mode bifurcation occurs. Thus, the H-mode theory discussed here is consistent with the experimental result that the condensed neutrals trigger the H-mode transition. The critical neutral density ξ^c is estimated in terms of ν_{*i} and d_n and its dependences on ν_{*i} and d_n are shown in Fig.18 and examined. The large neutral density near the X-point is found to be needed for the transition when the collisionality ν_{*i} or the neutral density d_n at the main plasma is increased. However, we emphasize that the key mechanism for the bifurcation is still the ambipolar condition including the loss cone loss and the anomalous loss. If this key mechanism is masked by the effects of neutrals at main plasma, the L/H transition would not occur. Conversely, if the key mechanism is unmasked by the effects of neutrals near X-point, the H-mode transition can occur. The critical pressure gradient for the L/H transition discussed here also alters if we choose the different values of ν_{*i} and d. The condition for the L/H transition is estimated. The parameter surveys are done. It is obtained that the critical λ value becomes larger when the collisionality ν_{*i} becomes large in the small d region. The change of the critical λ is found to become small when the value of ν_{*i} is varied from one to five in the large d region.

In Chapter 7, to include the effect of E'_r, we extended the ELM model equation based on the electric field bifurcation model for the L/H transition. The 0-D model was employed and a constant-ℓ approximation was done. The stationary solution of the dynamic equation, *i.e.*, the solution of Eq. (7.3), of high particle flux corresponds to the L-phase and that of low particle flux corresponds to the H-phase, respectively. The extended ELM model is composed of the temporal equations of the thermodynamic force λ and the loss rate D. The time dependent Ginzburg -Landau equation, which includes the nonlinear term in the E'_r transition model (see Fig.21), was formulated for the development of the loss rate D. Near the transition boundary of the L- and H-modes, a solution was obtained in which the self-generated oscillation of the outflux (Γ) and the thermodynamic force (λ) occurs under the constant influx (S) condition (see Fig. 23). We examined the dynamical stability of the stationary solution. The existence of the self-generated oscillation was confirmed also in the presence of E'_r. We also attribute this state to a kind of dithering ELMs in the presence of both E_r and E'_r. The form of the bursts depends upon the transition structure in the phase diagram like the one shown in Fig.21 and upon the trajectory which the plasma follows. The burst shape, therefore, alters if we choose the different values of d_0 and S. Also the choice of the constraint between E_r and E'_r strongly affects the curve, which is varied in experimental conditions. The details of the burst shape should be examined in accordance with the case of concern. The condition including the electric field shear for the occurrence of the self-generated oscillation was newly given. The parameter space corresponding to the condition (7.12) was also shown in Fig.24. It was found that the hatched region for the negative E'_r in the parameter space is wider than that for the positive E'_r. This asymmetry with respect to the sign of E'_r could be tested, In future, in the experiments like TEXTOR, in which sign of E'_r in the H-mode plasma can be controlled by external bias [5].

The condition of the L/H transition and of the appearance of the double hysteresis derived in this article critically depend on the assumption of the constant-ℓ model. Our model equation incorporates the local and stationary value of E'_r (sheared poloidal rotation) near the edge. In addition, throughout the article the zero-dimensional model is used to analyze the transition physics and the spatial structure is not solved. In reality, ℓ is not constant and the more precise form of Eq. (3.5) must be used to obtain the more exact condition. One way to resolve this problem is to solve the spatial-temporal evolution of the radial electric field near the edge. This is left for our future work.

The penetration of neutral particles to the edge region also affects the electric field structure. The effects of neutrals, *i.e.* the penetration depth, the neutral density and so on, on the structure are also left for future study.

With respect to the temporal evolution of the ELM bursts, the case with double hysteresis in the presence of an external source was not analyzed. There arises an interesting question whether chaotic dynamics would appear in the case of compound dithers.

In this article, we concentrate on the transition physics and do not discuss its impact on the anomalous transport. Only bipolar component of the flux is discussed for the H-mode transition. However, the energy flux could be dominated by the intrinsic ambipolar component of the flux [44]. The global energy confinement and the particle confinement could be discussed by summing up the ambipolar component, which are influenced by the jump of the radial electric field. The particle diffusivity of the bipolar component D^b_{e0} was taken to be a constant for simplicity, throughout this article. The inclusion of the parameter dependence of D^b_{e0} together with the analyses of the intrinsic ambipolar diffusion is also left for our future study. Furthermore, the couplings of the temperature development or to in different directions are neglected. The models for the heat conductivity χ (or the particle diffusivity D) have been proposed in many articles. As a candidate, the heat conductivity χ for the nonlinear self-sustained turbulence of the pressure driven modes was given in Refs. [59, 60] as

$$\chi=\frac{\chi_L}{1+G_1\omega^2_{E1}}, \tag{8.1}$$

where χ_L is the heat conductivity in the L-mode, the parameter ω_{E1} stands for the shear effect of the radial electric field and G_1 is the certain function of the pressure gradient and the magnetic shear parameter. The details are given in Refs. [59, 60]. Investigations on the heat conductivity in addition to that on the particle diffusion coefficient are necessary to understand the electric field structure at the L/H transition. These problems are left for the future study.

There are other mechanisms to induce bipolar losses. The electron ripple loss is an example. The existence of the other impurity ions also affects the bipolar loss. These may add a variety in the transition condition.

Regarding the effects of scrape-off plasmas, we neglect the ion loss cone loss of the ion orbit outside the separatrix surface. In order to examine this effects, the radial dependence of E_r across the separatrix should be taken into account. Furthermore, the electric field is not always constant along the magnetic field line outside the separatrix surface. Further analysis is necessary.

Table 1. Parameters in Chapter 1

electron charge	e
ion poloidal gyroradius	ρ_{pi}
radial electric field	E_r
ion temperature	T_i
	$X=e\rho_{pi}E_r/T_i$
ion-ion collision frequency	ν_{ii}
major radius	R
safty factor	q
ion thermal velocity	v_{Ti}
inverse aspect ratio	ε
effective collisionality	ν_{*i}
radial electric field shear	E'_r

Table 2A. Parameters in Chapter 2

plasma beta	β_p
line averaged electron density	$\bar{n}_e$
perpendicular plasma beta	$\beta_{p\perp}$
electron temperature	T_e
power of neutral injection	P_{NI}
injected power	P
threshold power of L/H transition	P^{LH}_{sep}
frequendcy of ELMs	ν_{ELM}
energy power through separatrix	P_{sep}
toroidal mode number	N
poloidal mode number	M
minor radius	a
toroidal magnetic field	B_t
numerical coefficient	$F(0<F<1)$
ion density	n_i
ion loss	Γ_i
ion parallel velocity	$v_{\parallel}$
ion distribution function	f_i
loss cone loss of ions	Γ_i^{lc}
numerical coefficient	$\hat{F}$
anomalous loss	Γ^{anom}_{e-i}

Table 2B. Parameters in Chapter 2

numerical coefficient	α
bipolar anomalous diffusivity	D^b_{e0}
normalized particle flux	$\hat{\Gamma}$
	$d_0=D^b_{e0}\sqrt{\varepsilon}/(\rho^2_{pi}\hat{F}\nu_i)$
	$\lambda=-\rho_{pi}(n'_e/n_e+\alpha T'_e/T_e)$
critical value of λ	λ_c
poloidal flow velocity	U_p
poloidal magnetic field vector	$\mathbf{B}_p$
ion viscosity tensor	$\overleftrightarrow{\pi}$
poloidal (pararell) vicosity	$\langle \mathbf{B}_p \cdot \nabla \cdot \overleftrightarrow{\pi} \rangle$
ion mass	mi
radial coordinate	r
ion gyroradius	Pi
	$U_{p0}=-\rho_i(dT_i/dr)/T_i$
integral quantity	I_p
integral quantity	I_T
particle velocity	v
	$x=v/v_{Ti}$
poloidal magnetic field	B_p

Table 2C. Parameters in Chapter 2

magnetic field	B
	$U_{p,m}=U_pB/(v_{Ti}B_p)+\lambda/2$
geometric factor	G
numerial coefficient	ω
chracterisitic width	Δr
light velocity	c
magnetic field vector	$\mathbf{B}$
ion loss cone loss vector	Γ_i^{lc}
left side of Eq. (2.10)	$Y_1(U_{p,m})$
right side of Eq. (2.10)	$Y_2(U_{p,m})$
j which denotes ions (i) or electrons (e)	j
particle flux due to bulk viscosity	Γ_j^{bv}
numerial coefficient	γ_i
neoclassical particle diffusivity	D_j
Larmor radius	$\rho_j=\sqrt{2m_jT_j}/(eB)$
mean velocity along magnetic field	$U_{j\parallel}$
ambipolar electric field	E_a
	$X_a=e\rho_{pi}E_a/T_i$

Table 2D. Parameters in Chapter 2

ion pressure	$P_i=n_iT_i$
poloidal electric field	E_p
Pfirsch-Schülter radial loss	$\Gamma_i^{P.S.}$
mean free path	λ_{mfp}
	$\Theta=B_p/B$
	$y=qR/\lambda_{mfp}$
plasma dispersion function	$Z(X,y)$
dielectric constant of vacuum	ε_0
perpendicular dielectric constant of magnetized plasma	$\varepsilon_\perp$
loss of ions due to collisions between ions and neutrals	Γ_i^n
loss of ions from other collisional processes	Γ_i^{NC}
loss of electrons from other collisional processes	Γ_e^{NC}
time after L/H transition	$\triangle t$
intesity of SX radiation	I
radial position of separatrix	r_s
current due to loss cone loss	j^L
current due to bulk viscosity loss	j^N

Table 3. Parameters in Chapter 3

hot ion loss due to toroidal rippled field	Γ_i^{rp}
numerical constant	$C_{rp}(=12.38)$
toroidal ripple	δ
subscript which represents hot ion component	h
neutral density	n_0
collision cross section	σ
numerical coeffieient	α_i
radial extent of transport barrier	ℓ
numerical correction	C
	$u_g=\rho_{pi}E'_r/(v_{Ti}B_p)$
bipolar part of effective diffusivity in presence of E'_r	D_e^b
critical parameter which satisfies $u_c^2=8\sqrt{2\varepsilon}\,(4-u_c)$	u_c
angular frequency	ω
Doppler shifted angular freaquency	$\omega_E=ME_r/(rB)$
angular frequency of the mole	$\tilde{\omega}=\omega+\omega_E$

Table 4. Parameters in Chapter 4

ion (electron) density if $n_i=n_e$	n
ion (electron) temperature if $T_i=T_e$	T
	$d=D_{e0}^b/(\sqrt{\varepsilon}\,\omega_b\rho_{pi}^2)$
	$\lambda_h=-\rho_{pi}n'_h/n_h$
density of bulk ions	n_{i0}
	$r_n=n_{i0}/n_i$
second term in left hand in Eq. (4.1)	$\hat{\Gamma}_i^{rp}$

Table 5. Parameters in Chapter 5

effective loss rate	D
source	S
small parameter	$v\sim O(B_p^2/B_t^2)$
	$\hat{D}(\lambda)\equiv\hat{\Gamma}/\lambda$
Alfvén velocity	v_A
value of $\hat{D}$ at points $A, B, \cdots$ in Fig.11 (a)	$\hat{D}(A, B, \cdots)$
value of λ at points $A, B, \cdots$ in Fig.11 (a)	$\lambda(A, B, \cdots)$
loss flux	$\Gamma(=D\lambda)$

Table 6. Parameters in Chapter 6

collisional frequency of trapped ions	$\nu_{in_0^X}$
effective detrapping frequency	$\nu_{eff}(=\nu_{ii}+\nu_{in_0^X})$
	$d_n=n_0^{main}\langle\sigma v\rangle(1+2q^2)/(\sqrt{\varepsilon}\,\omega_b q^2)$
neutral density at midplane	n_0^{main}
	$\xi=\nu_{in_0^X}/\omega_b$
neutral density near X-point	n_0^X
lower limit of ξ for multiple solution	ξ^*
lower limit of ξ for L/H transition	ξ^c

Table 7A. Parameters in Chapter 7

	$\lambda_r=\lambda-\rho_{pi}(eBr\omega/(MT_e))$
poloidal fluid velocity	u_p
toroidal fluid velocity	u_t

Table 7B. Parameters in Chapter 7

value of λ where H→L transition occurs	λ_1
value of λ where L→H transition occurs	λ_2
value of $\hat{D}$ where H→L transition occurs	D_1
value of $\hat{D}$ where L→H transition occurs	D_2
	$\zeta=u_g/u_c$
influx	Γ_{in}
typical value of density in L-mode	n_L
	$g_1=/n_L$
	$g_2=\lambda_2/n_L$
effective diffusivity	D
numerical coefficients	β_1, β_2
typical of effective diffusivity invalu L-mode	D_L
typical value of gradient parameter in L-mode	λ_L
fundamental source	S_0
amplitude of external oscillation	ε_f
frequency of external oscillation	Ω

Table 8. Parameters in Chapter 8

heat conductivity	χ
heat conductivity in L-mode	χ_L
shear effect of radial electric field	ω_{E_1}
function of pressure gradient and magnetic shear parameter	G_1

Acknowledgement

First of all, the author would like to thank to the help and the encouragement of all personnels and graduate students of the Interdisciplinary Graduate School of Engineering Sciences and Research Institute for Applied Mechanics, Kyusyu University. He expresses his gratitude to the following people for their special contributions.

The author would like to express his sincerest gratitude to Professor S. -I. Itoh for her guidance, support and encouragement throughout this work. He is indebted to Professor K. Muraoka and Professor H. Zushi for their useful advise and criticism in revising of the manuscript.

He also wishes to express his deep appreciation to Associate Professor M. Yagi for stimulating discussions and continuous encouragement. Special thanks are also extended to Professor K. Itoh (National Institute for Fusion Science), Associate Professor A. Fukuyama (Okayama University) and Dr. Y. Miura (Japan Atomic Energy Research Institute) for their kind advise and the creative comment.

Furthermore, the author is grateful to the graduated and the current students who collaborated and studied with him in his laboratory; Messrs. T. Kubota, G. Tateishi, T. Iwasaki, T. Fujimoto and N. Yamamoto. Thanks are also expressed to Messrs. K. Ueno, K. Yabuki, H. Yamaguchi and T. Aoyagi.

This work is partly supported by RA (Research Assistant) fellowship in collaboration with the Advanced Fusion Research Center of Kyusyu University and JSPS Research Fellowships for Young Scientists.

Finally, the author wishes to thank his family.

References

[1] F. Wagner, G. Becker, K. Behringer, *et al.*, Phys. Rev. Lett. **42** (1982) 1408.

[2] K. H. Burrel and DIII-D Group, *Proc. 12th. Int. Conf. on Plasma Physics and Controlled Nuclear Fusion Research, Nice, 1988* (*IAEA, Vienna, 1988*), Vol 1, p93.

[3] JET TEAM, *Proc. 12th. Int. Conf. on Plasma Physics and Controlled Nuclear Fusion Research, Nice, 1988* (*IAEA, Vienna, 1988*), Vol 1, p261.

[4] R. J. Taylor, M. L. Brown, B. D. Fried *et al.*, Phys. Rev. Lett. **63** (1989) 2365.

[5] R. R. Weynants, G. v. Oost, G. Bertschinger *et al.*, Nucl. Fusion **32** (1992) 837.

[6] L. G. Askinazi, V. E. Golant, S. V. Lebedev, V. A. Rozhanskij and M. Tendler, Nucl. Fusion **32** (1992) 271.

[7] R. R. Groebner, K. H. Burrel and R. P. Seraydarian, Phy. Rev. Lett. **64** (1990) 3015.

[8] S. -I. Itoh and K. Itoh, Phys. Rev. Lett. **60** (1988) 2278.

[9] S. -I. Itoh and K. Itoh, Nucl. Fusion **29** (1989) 1031.

[10] K. C. Shaing and E. C. Crume Jr., Phys. Rev. Lett. **63** (1989) 2369.

[11] K. C. Shaing, E. C. Crume Jr. and W. A. Houlberg, Phys. Fluids **B2** (1990) 1492.

[12] K. C. Shaing, Phys. Fluids **B4** (1992) 290.

[13] A. B. Hassam, T. M. Antonseck, Jr., J. F. Drake and C. S. Liu, Phys. Rev. Lett. **66** (1991) 309.

[14] T. E. Stringer, Nucl. Fusion 33 (1993) 1249.
[15] K. Itoh and S. – I. Itoh, Nucl. Fusion **32** (1992) 2243.
[16] P. H. Diamond, Y. – M. Liang, B. A. Carreras and P. W. Terry, Phys. Rev. Lett. **72** (1994) 2565.
[17] H. Sugama and W. Horton, Phys. Plasmas **1** (1994) 345.
[18] P. H. Diamond, V. Shapiro, V. Shevchenko *et al., Proc. 14th. Int. Conf. on Plasma Physics and Controlled Nuclear Fusion Research, Würzburg, 1993 (IAEA, Vienna, 1994)*, Vol 2, p97.
[19] F. L. Hinton, Phys. Fluids **B3** (1991) 696.
[20] S. -I. Itoh and K. Itoh, J. Phys. Soc. Jpn. **59** (1990) 3815; S. -I. Itoh and K. Itoh. *Proc. 13th. Int. Conf. on Plasma Physics and Controlled Nuclear Fusion Research, Washington, DC, 1990 (IAEA, Vienna, 1991)*, Vol 2, p321.
[21] Y. Miura, H. Akikawa, K. Hoshino *et al., Proc. 13th. Int. Conf. On Plasma Physics and Controlled Nuclear Fusion Research, Washington, DC, 1990 (IAEA, Vienna, 1991)*, Vol 1, p325.
[22] ASDEX Team, Nucl. Fusion **29** (1990) 1959.
[23] DIII-D Team, *Proc. 13th. Int. Conf. on Plasma Physics and Controlled Nuclear Fusion Research, Washington, DC, 1990 (IAEA, Vienna, 1991)*, Vol. 1, p.629.
[24] T. Shoji and JET-2M Group, *Proc. 17th European Conf. on Controlled Fusion and Plasma Physics, Amsterdam, 1990 (European Physics Society, Amsterdam, 1990)*, Part III, p1452.
[25] M. Keihacker, G. Becker, K. Bernhadi *et al.*, Plasma Phys. Control. Fusion **26** (1984) 49.
[26] T. H. Osborne, K. H. Burrel, T. Carlstrom *et al.*, Bull. Am. Phys. Soc. **35** (1990) 1975.
[27] S. -I. Itoh, K. Itoh and A. Fukuyama, Y. Miura and JFT-2M Group, Phys. Rev. Lett. **67** (1991) 2505.
[28] S. -I. Itoh, K. Itoh and A. Fukuyama, Nucl. Fusion **33** (1993) 445.
[29] H. Zohm, ASDEX-Upgrade Team and NI and ICRH Group, Phys. Rev. Lett. **72** (1994) 222.
[30] H. Zohm, K. Büchl, A. R. Field, J. C. Fucks, O. Gehre, A. Herrmanm, M. Kaufmann, G. Lieder, F. Ryter, M. Schittenhelm, ASDEX-Upgrade Team and ICRF-Group, *Proc. 20th. European Conf. on Controlled Fusion and Plasma Physics, Genova 1993 (European Physics Society, Genova, 1993)* Part I, p 23.
[31] H. Zohm, Plasma Phys. Control. Fusion **38** (1996) 105.
[32] R. D. Hazeltine, Phys. Fluids **B1** (1989) 2031.
[33] S. P. Hirshman and D. J. Sigmar, Nucl. Fusion **21** (1981) 1079.
[34] H. L. Berk and A. A. Galeev, Phys. Fruids **10** (1967) 441.
[35] R. D. Hazeltine, Bull. Am. Phys. Soc. **33** (1988) 2107.
[36] A. A. Galeev and R. Z. Sagdeev, Sov. Phys. JETP **26** (1968) 233.
[37] T. E. Stringer, Nucl. Fusion **32** (1992) 1421.
[38] J. W. Connor and T. E. Stringer, Phys. Fluids **14** (1971) 2177.
[39] J. W. Connor and T. E. Stringer, Phys. Fluids **14** (1971) 2184.
[40] B. M. Fried and S. D. Conté, The Plasma dispersion function, Academic Press, New York and London (1961)
[41] J. W. Connor and R. J. Hastie, Phys. Fluids **17** (1973) 114.
[42] K. C. Shaing and C. T. Hsu, Phys. Plasmas **2** (1995) 1801.
[43] See, for a review, *e.g.*, K. Itoh, Plasma Phys. Control. Fusion **36** (1994) A307.
[44] K. Itoh and S. -I Itoh, Plasma Phys. Control Fusion **38** (1996) 1.
[45] S. -I. Itoh, K. Itoh and A. Fukuyama, 'ELMy-H mode as Limit Cycle and Chaotic Oscillations in Tokamak Plasmas', National Institute for Fusion Science Report, NIFS-**96**.
[46] K. C. Shaing, Phys. Fluids **31** (1988) 2249.
[47] B. A. Carreras, K. Sidikman, P. H. Diamond, P. W. Terry and L. Garcia, Phys. Fluids **B4** (1992) 3115.
[48] Y. Z. Zhang and S. M. Mahajan, Phys. Fluids **B5** (1990) 2000.
[49] T. S. Hahm and W. M. Tang, Phys. Plasmas **1** (1994) 2049.
[50] M. Kikuchi *et al., Proc. 14th. Int. Conf. on Plasma Physics and Controlled Nuclear Fusion Research, Würzburg, 1992 (IAEA, Vienna, 1992)* Vol. 1, p189.
[51] S. Toda et al., Trans. of Fusion Technology **27** (1995) 489.
[52] S. Toda, S. -I Itoh, M. Yagi, A. Fukuyama and K.

Itoh, *Proc. 22nd. European Conf. on Controlled Fusion and Plasma Physics, Bournemouth 1995* (*European Physics Society, Bournemouth 1995*) Part I, p205.

[53] S. Toda, M. Yagi, S. -I. Itoh, A. Fukuyama and K. Itoh, Plasma Phys. Control Fusion **38** (1996) 1337.

[54] Y. Miura *et al.,* submitted to Plasma Phy. Control Fusion.

[55] S. Toda, S. -I Itoh, M. Yagi and Y. Miura, Plasma Phys. Control. Fusion **39** (1997) 301.

[56] S. Toda, S. -I Itoh, J. Phys. Soc. Japan **65** (1996) 1284.

[57] R. D. Hazeltine and F. L. Hilton, Phys. Fluids **16** (1973) 1883.

[58] N. Ueda, K. Itoh and S. -I. Itoh, Nucl. Fusion **29** (1989) 173.

[59] K. Itoh, S. -I. Itoh, A. Fukuyama, M. Yagi and M. Azumi, Plasma Phys. Control Fusion **36** (1994) 279.

[60] S. -I Itoh, K. Itoh, A. Fukuyama and M. Yagi, Phys. Rev. Lett. **72** (1994) 1200.